

POLITECNICO DI TORINO

Master Degree in Biomedical Engineering

**Computational Investigation of Ska Complex-Tubulin Molecular
Interactions to Shed Light on Force Generation Mechanisms in
Kinetochore-Microtubule Junctions**



Thesis Supervisor

Prof. Jack Adam Tuszynski

Co-supervisor

Prof. Marco A. Deriu

Candidate

Hedyeh Khoshkhoo Gilvaei

ACADEMIC YEAR 2018-2019

Sommario

Sommario.....	1
ABSTRACT.....	4
1 INTRODUCTION	5
2 SCIENTIFIC BACKGROUND	7
2.1 MICROTUBULES.....	7
2.1.1 Functions of microtubules	7
2.1.2 Tubulin dimers	7
2.1.3 Microtubule architecture.....	8
2.1.3 Microtubule polymerization	9
2.2 MITOSIS IN EUKARYOTIC CELLS.....	11
2.2.1 Chromosomes dynamics in mitosis	11
2.2.1 Role of microtubules during mitosis.....	12
2.3 SKA COMPLEX.....	13
2.3.1 Chromosome-microtubule interaction.....	13
.....	16
2.3.2 Ska complex structure and functions	16
2.3.3 Interaction characteristics of Ska complex with microtubules	18
2.3.4 Ska-1 microtubule binding domain.....	19
2.4 FORCE GENERATION MECHANISMS IN KINETOCHORE-MICROTUBULE JUNCTIONS.....	22
2.4.1 Hydrolysis cycles and polymerization of tubulin	22
2.4.2 Force generation by depolymerizing microtubules.....	23

2.4.3	Force Generation within the Microtubule Lattice	25
3.	METHODS.....	27
3.1	Computational molecular modeling	27
3.2	Molecular Dynamics.....	29
3.2.1	The potential energy function.....	31
3.2.2	Periodic boundary conditions	34
3.2.3	Treatment of the non-bond interactions	35
3.2.4	Simulated ensembles in molecular dynamics	37
3.2.5	Steered Molecular Dynamics.....	39
3.3.4	Software packages.....	43
4.	TUBULIN-SKA INTERACTION CHARACTERIZATION BY MOLECULAR	44
	MODELLING WITH ATMOIC RESOLUTION	44
4.1	INTRODUCTION	44
4.2	MATERIALS AND METHODS	46
4.2.1	System set up.....	46
4.2.2	Simulation Setup.....	48
4.3	RESULTS	48
4.3.1	Conformational Analysis.....	48
4.3.2	Interaction probability analysis	53
4.3.3	Steered Molecular Dynamics.....	56
4.4	DISCUSSION	57
5	CONCLUSIONS	58

6 Acknowledgments.....	60
7 References	61

ABSTRACT

Microtubules (MTs) are involved in several cellular processes and play a key role during mitosis, forming the mitotic spindle which is able to divide the chromosomes. The connection between microtubules and chromosomes is guaranteed by a macro structure including various motor proteins, called *kinetochore*. Microtubule instability, characterized by lengthening and shortening of the MTs, generates forces at the kinetochore, that lead the chromosomes toward the metaphase plate. Therefore, the stability of the junctions between kinetochore and plus end of the microtubule is a critical issue for an accurate chromosome segregation. The stability of the kinetochore-microtubule interaction is guaranteed by a W-shaped homodimer of coiled coils, called *ska complex*, which is crucial for a correct cell division in human cells: the MT-binding domains (MTBDs) of the *ska* complex recognizes tubulin monomers making transversal bindings. However, molecular mechanisms at the basis of the interaction between tubulin and *ska* complex is not completely understood yet.

In this research, computational molecular docking has been employed to determine most likely three-dimensional configurations of *ska* complex docked to $\alpha\beta$ tubulin heterodimer. Moreover, molecular phenomena induced by Ska1-MT Binding Domain (experimentally known) interaction have been deeply investigated by molecular modelling techniques with atomic resolution. In particular, classical and steered Molecular Dynamics were employed to highlight the most favorable protein-protein complex configuration and to investigate the force generation mechanism in the kinetochore-microtubule junctions. Future studies might consider binding interactions between *ska* complex and ring protofilaments or an entire piece of microtubule wall to shed light on force generation mechanisms driving the whole segregation process of chromosomes in human cell.

1 INTRODUCTION

The mechanisms that govern the cell mitosis and the accurate chromosome segregation, has been one of the fundamental issues for the scientists over decades. The mitotic spindle which is the key element for chromosome alignment procedure, is composed of a complex combination of microtubules especially in higher eukaryotic cells. Microtubules are cytoskeletal structures involved in several cell functions and are constituted of the $\alpha\beta$ heterodimers, arranged in a head-to-tail style to form linear protofilaments. These protofilaments bound laterally to form a hollow cylindrical polymer. The dynamic instability of microtubules conceives the driving forces for chromosome movements in the context of mitotic spindle. The instability of microtubules cap is also a critical issue for accurate chromosome alignment, this issue is controlled by a macromolecular structure consisting of various motor proteins called *kinetochore* which is responsible for maintenance of stable connections of highly active microtubule caps with chromosomes. Therefore, proper chromosome segregation depends on the stability of the kinetochore-microtubule junctions. The stability of kinetochore-microtubule interactions is guaranteed by a W-shaped homodimer of coiled coils, called *Ska complex*, which is vital for a correct cell division in human cells. The microtubule binding domains (MTBDs) of the ska complex attaches tubulin monomers making transversal bindings.

In recent years, the computational investigations have employed in enormous researches to optimize the calculations and particularly are utilized in biological systems including huge number of molecules. Computational Molecular Modeling furnishes a variety of methods such as Molecular Dynamic (MD) or Steered Molecular Dynamic (SMD), for analyzing the mechanical properties of biological systems with atomic resolution.

The purpose of this research is to underline the most favorable protein-protein complex of microtubule binding domains of ska complex bounded to $\alpha\beta$ tubulin heterodimer and to explore the mechanism of the force generation in the kinetochore-microtubule junctions.

The thesis is divided in the following sections.

Chapter 1 is the present introduction.

Chapter 2 is dedicated to scientific background declaring the mechanisms and elements which organize mitosis cell segregation, describing the fundamentals of microtubules characteristics, kinetochore structural elements and particularly declaring the role of ska complex in the chromosome alignments, finally the biophysical background on the mechanics of force generation in microtubules.

Chapter 3 is an overview of the methods used in this work. Molecular mechanics and molecular dynamics are described in general, focusing on physical and theoretical aspects.

Chapter 4 is assigned to molecular modelling of ska-tubulin complex with atomic resolution employing classic and steered molecular dynamics, succeeded by the conformational analysis of the structures after molecular dynamics and inspection on interaction probability of tubulin binding domains of ska. At the end an examination on the elasticity of the ska and the strength of the interactions between ska and tubulin heterodimer has been carried out.

2 SCIENTIFIC BACKGROUND

2.1 MICROTUBULES

Microtubules are fundamental components of cells which perform various tasks in cellular procedures. They constitute the structure of mitotic spindle which perform a key role in cellular mitosis¹⁻³. Microtubules are composed of $\alpha\beta$ -tubulin heterodimers and their polymerization and depolymerization are the principal process which affect the cell hemostasis^{4,5}.

2.1.1 Functions of microtubules

Microtubules are the cytoskeletal filaments in eukaryotic cells which involve in several cellular processes. They are responsible to support cellular structure in order to organize the cell shape and preventing undesired configurations⁶. Another important role of microtubules is the interaction with motor proteins for example kinesin and dynein, the microtubules play as pathways for the transportation of such motor proteins⁷.

One of the important functions of microtubules is the intervention in mitosis cellular division. Microtubules constitute a cylindrical structure called mitotic spindle which is fundamental in chromosomes alignment toward poles leading the cell segregation^{1,2,7-9}. The *dynamic instability* of microtubules that alternate between cycles of growth and rapid shrinkage, preserves the functionality of these filaments in cellular segregation. The polymerization and depolymerization of microtubules initiate mechanical forces which separate the chromosomes.

2.1.2 Tubulin dimers

The building blocks of the microtubules are $\alpha\beta$ -tubulin heterodimers which are constituted by two globular proteins, α and β tubulin monomers. The structure of α and β tubulin are very similar, they have 40% sequence identity in their amino acid arrangements. The weight of each monomer is about 50 kDa. Each monomer is bounded to a guanine nucleotide. Both tubulin monomers have a close-packed structure, but it can be divided three functional domains: the amino terminal domain including the nucleotide binding sites, the intermediate domain and the

carboxy-terminal domain. The N-terminal domain composed of residues (1-205), comprise a Rossman fold, a representative form of nucleotide binding proteins. The intermediate domain contains residues (206-381) following with the C-terminal residues (384-444)¹⁰⁻¹². Exposed to solvent, guanosine-5'-triphosphate (GTP) and guanosine-5'-diphosphate (GDP) are bound to tubulin monomers. The nucleotide bound to α -tubulin is nonexchangeable considering its position in the interface of tubulin monomers, instead on the β -tubulin nucleotide located on the monomer surface can hydrolyze called exchangeable^{10,13}.

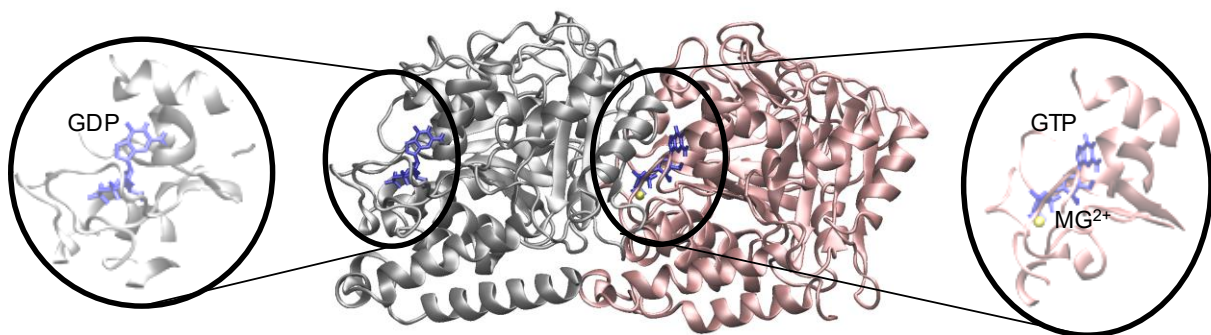


Figure 2.1 Tubulin heterodimer demonstrated as α -tubulin (right) and β -tubulin (left). GTP and GDP nucleotides are bonded to alpha and beta tubulin, respectively.

2.1.3 Microtubule architecture

Microtubules are cylindrical protein filaments with an external diameter of around 25 nm and an internal diameter of about 18 nm. Microtubules are made up of $\alpha\beta$ tubulin heterodimers, which organize a two dimensional sheet of tubulin in a three start helical structure^{12,14-16}. The alpha subunits tend to link a beta in the longitudinal direction and an alpha in circumferential direction¹⁵.

The $\alpha\beta$ heterodimer is very steady and the dimers connect head to tail to develop a protofilament. The protofilaments combine laterally creating a tube-like conformation; the offset between dimers of adjacent protofilaments is about 0.92 nm, so the total offset between the first

and the last protofilament is equal to the length of three monomers. This results a 3-start helical structure, while the protofilaments are parallel to the microtubule axis^{12,14-16}.

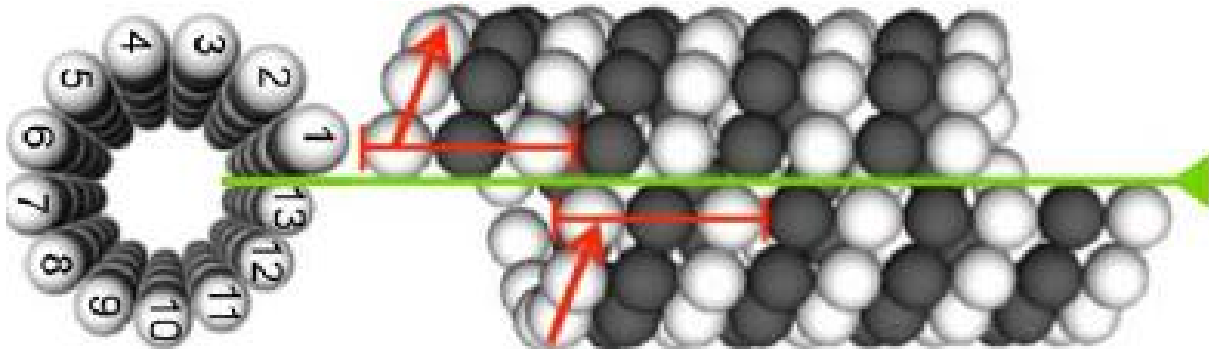


Figure 2.2 Three-start helical structure of eukaryotic microtubule¹⁷

2.1.3 Microtubule polymerization

By incorporation of α and β monomers on the plus end of microtubule, polymerization initializes. The α -tubulin is located on the minus end and β -tubulin is located on the plus end of microtubule. Tubulin monomers before incorporating to the microtubule bind to GTP molecule, this can hydrolyze in the microtubule lattice after polymerization. But if these GTP bounded monomers locate at the end of microtubule can remain in GTP state and conform a GTP-cap. The microtubule instability derives from the fact that GTP bound tubulin monomers are favorable to polymerizing and GDP bound instead tend to break up. Therefore, depolymerization initializes where GTP-cap is lost, this debilitates interactions at GDP-tubulin leading the protofilament to flare out^{18,19}.

Microtubules in vitro and in vivo demonstrate a non-equilibrium behavior and shift between phases of growth and shrinkage. This is called *dynamic instability*. Stochastic passage from growing to shrinkage is called catastrophe while transition from shrinkage to growing named

rescue. This feature creates a critical function: the “capture” of kinetochore during the prophase of mitosis. During mitosis, microtubules polymerize in random directions from any spindle pole and could be stabilized if catch the kinetochore, if not, endure a catastrophe and shrink back to the pole, then other microtubules start to elongate in random directions^{4,5,16,19–22}. The minus end of microtubule is attached to centrosome while the very unstable plus end endure the stochastic transitions.

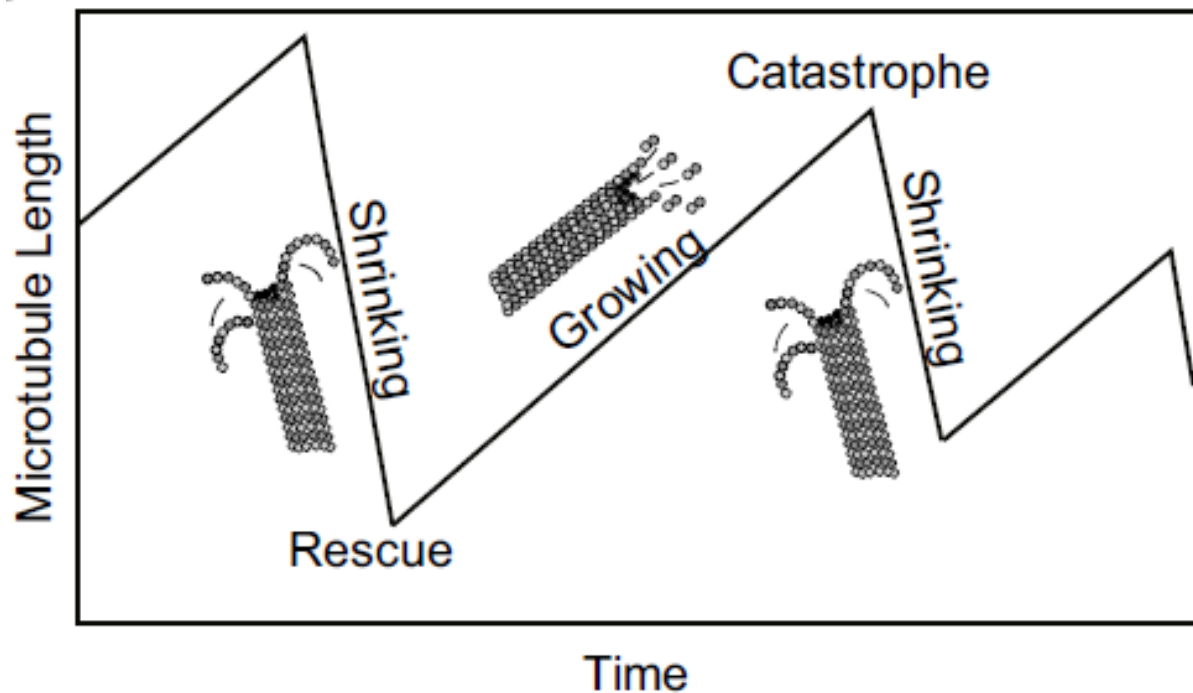


Figure 2.3 Microtubule growth and shrinkage, transitions through catastrophe and rescue constitute dynamic instability of microtubules¹⁹.

2.2 MITOSIS IN EUKARYOTIC CELLS

2.2.1 Chromosomes dynamics in mitosis

Mitotic cell division is a vital process by which organisms survive and it is the final step of the cell cycle. During mitosis the genetic material divide equally between two new daughter cells. It has been defined five steps of this segregation process in eukaryotic cells:

1. Prophase: Duplicated Centrosomes move around the nucleus and the chromosomes condensate.
2. Prometaphase: In this stage the nuclear envelope starts to break down conceding the interaction between the kinetochores and microtubules, so chromosomes move towards the spindle equator.
3. Metaphase: The whole amounts of chromosomes arrayed at the equator and develop a metaphase plate.
4. Anaphase: The sister chromatids turn away during anaphase until finding their new positions at the mitotic spindle poles.
5. Telophase: During this step, the chromosomes which are positioned at the spindle poles begin to decondense. In addition, nuclear envelope starts covering these decondensing chromosomes in order to create daughter nuclei^{1,8}.

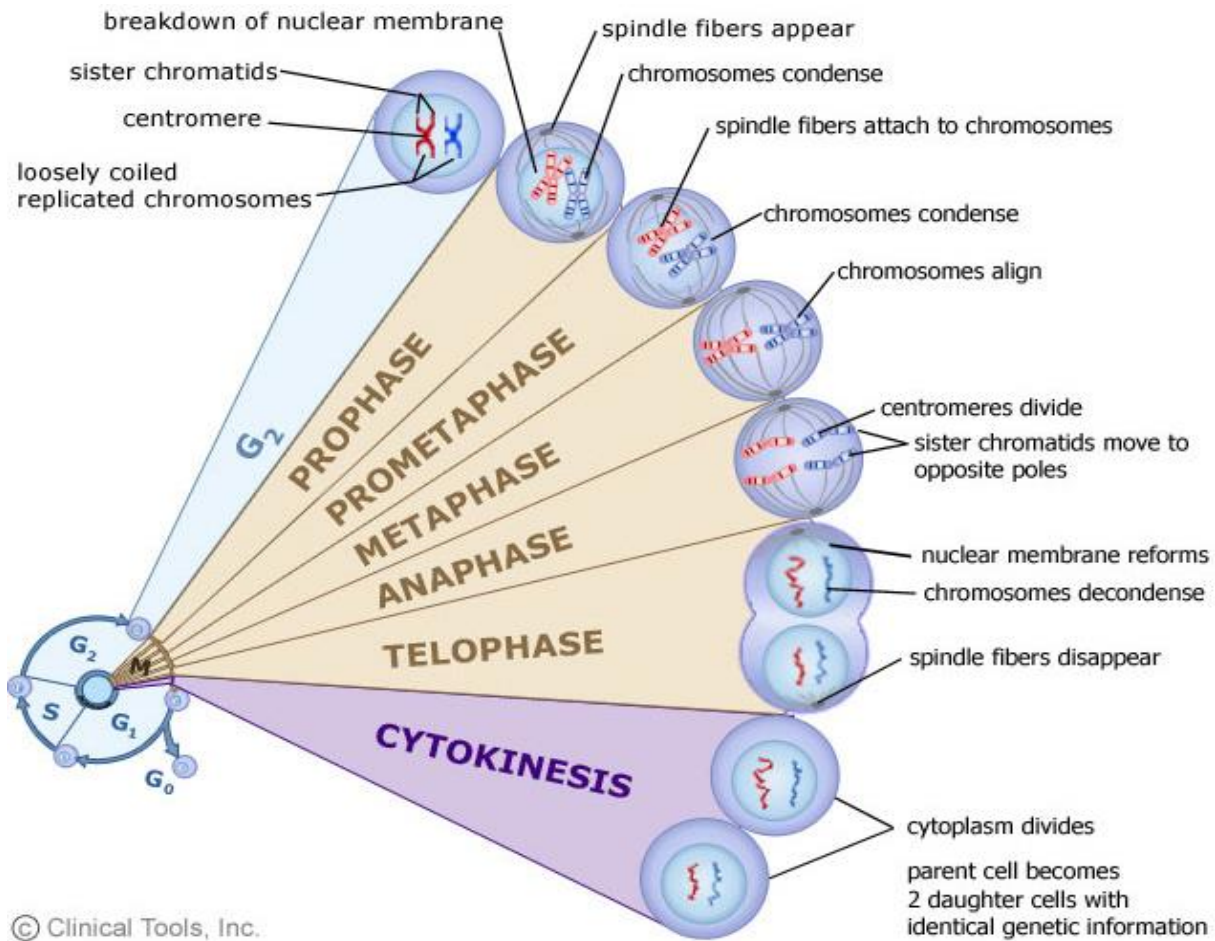


Figure 2.4 The cell cycle (<https://www2.le.ac.uk/projects/vqec/highereducation/topics/cellcycle-mitosis-meiosis>)

2.2.1 Role of microtubules during mitosis

Mitotic spindle is a complex structure which perform chromosome segregation during mitosis. It is composed of microtubules, hollow cylindrical polar filaments with a fast growing plus end containing β -tubulin and a slow growing minus end including α -tubulin monomer^{5,22,23}. The dynamic instability of microtubules is the driving force of chromosome segregation. Microtubules are divided in three different categories: kinetochore microtubules, non-kinetochore (called also interpolar) and astral microtubules. Kinetochore microtubules lead the chromosomes motion in

anaphase, these microtubules are connected to kinetochore at one end. They are also critical for chromosome arrangement during prometaphase and metaphase. In general kinetochore microtubules connect to non-kinetochore microtubules to reach the kinetochore but some of kinetochore microtubules elongate from centrosome to kinetochore. Astral microtubules emanate from the poles of mitotic spindle and are employed to position the spindle^{2,19}.

Successful mitotic division depends on the attachment of the mitotic chromosomes to the plus ends of microtubules. These attachments are performed by the interference of kinetochore. Proper chromosome segregation depends on the stability of the kinetochore-microtubule junctions, kinetochores must establish stable attachments to highly dynamic tips of microtubules which is a very important issue in mitosis procedure^{1,23-25}.

2.3 SKA COMPLEX

2.3.1 Chromosome-microtubule interaction

The attachment between microtubules and chromosomes is fixed by a structure composed of motor proteins, named kinetochore. In homo sapience cell, each 12-30 arrays of MTs finish to connect a single *kinetochore*. The plus end instability of MTs considered to be the driving forces for chromosome movements²⁶⁻²⁸. Genetic analysis confirmed that microtubule dynamics is the primary driving force of chromosome movement. In vitro experiments can estimate that the force generating by a single depolymerizing microtubule is about 30-65 pN. Classic experiments executed in grasshopper spermatocytes, had estimated that the force required to stall a chromosome is about 700pN, but recently using an optical trap in the same experiment the force was estimated to be 100 times lower. New in vivo measurements are necessary to clarify this great difference²⁹.

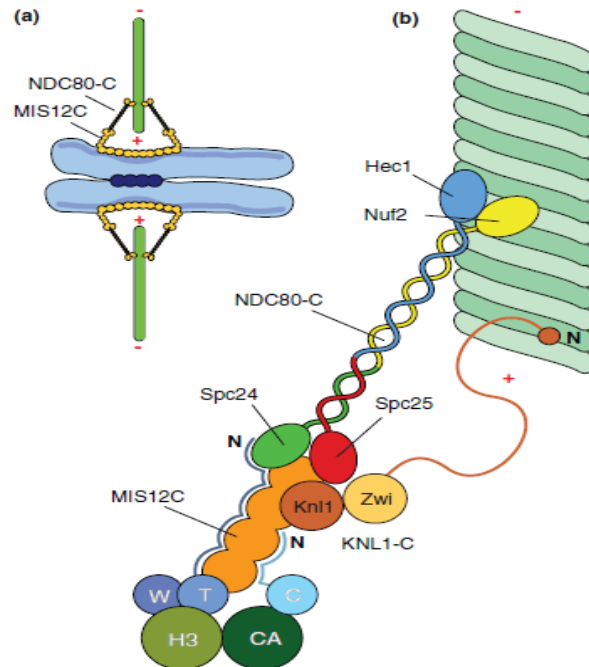


Figure 2.5 (a) while mitosis goes ahead the coherency of sister chromatids at centromeres is guaranteed (dark blue circles). The cluster of kinetochores (orange) on centromeric chromatin makes connections with microtubules (green). The plus (+) and minus (-) ends of microtubules are indicated. (b) kinetochore microtubule binding ²⁶.

The figure 2.5, illustrates how kinetochore protein group links to a MT. A group of 10 different kinetochore proteins, called KMN 'network', perform this connection. KMN network consists of **K**NL1 complex (KNL1-C, composed of Knl1/Spc105/Blinkin/CASC5/AF15q14 and Zwint-1), the **M**IS12 complex (MIS12-C, composed of Mis12/Mtw1, Dsn1, Nsl1, and Nnf1), and the **N**DC80 complex (NDC80-C, composed of Ndc80/Hec1, Nuf2, Spc24, and Spc25). The NDC80 complex has a tetrameric structure consisting at one termination, Spc24 and Spc25 subunits which face the MIS12-C, while the Hec1 and Nuf2 subunits interact with microtubule. The coiled-coil filament which connects globular fields of Hec1 and Nuf2 to the globular fields of Spc24 and Spc25 is about 60nm long. Ndc80 complex interacts at the dimeric interface of α - and β -tubulins and affects MT dynamics by supporting straight MTs^{26-28,30-33}.

Kinetochores assemble on the constitutive centromere associated network (CCAN) and arrest the plus end of the MT²⁷. Lengthening and shortening of the MTs originate from dynamic instability of the MTs, creating forces at the kinetochore that move the chromosomes toward the metaphase plate. But which factors guarantee the stability of the junctions between kinetochores and plus ends of MTs? We have already mentioned the role of the Ndc80 complex. It is a dumbbell-like structure about 570 Å long with tubulin binding sites at one terminal and kinetochore binding domains at the other end³⁴. The N-terminal of Hec1 and Nuf2 interact with the $\alpha\beta$ tubulin dimeric interface (called the 'toe print') with calponin homology (CH) (called the 'toe'). A pair of Hec1 and Nuf2 bound to $\alpha\beta$ tubulin heterodimer. This is the reason why Ndc80 prefers straight conformations of MT protofilaments²⁶.

Another component necessary for the establishment of stable kinetochore-microtubule interactions is a W-shaped homodimer of coiled coils, called *Ska complex*, which is vital for a correct cell division in human cells, and it is suggested to be an analogue of the Dam1/DASH complex in metazoans^{34,35}. The Ska complex needs Ndc80 to be oriented on the MTs and to be located on the kinetochores. The Ska complex is employed by the kinetochore by means of the KMN network and together with Ndc80 composes a united MT-binding machine. In fact, without Ndc80 the attachment between microtubules and kinetochores will be defective³⁴⁻³⁷.

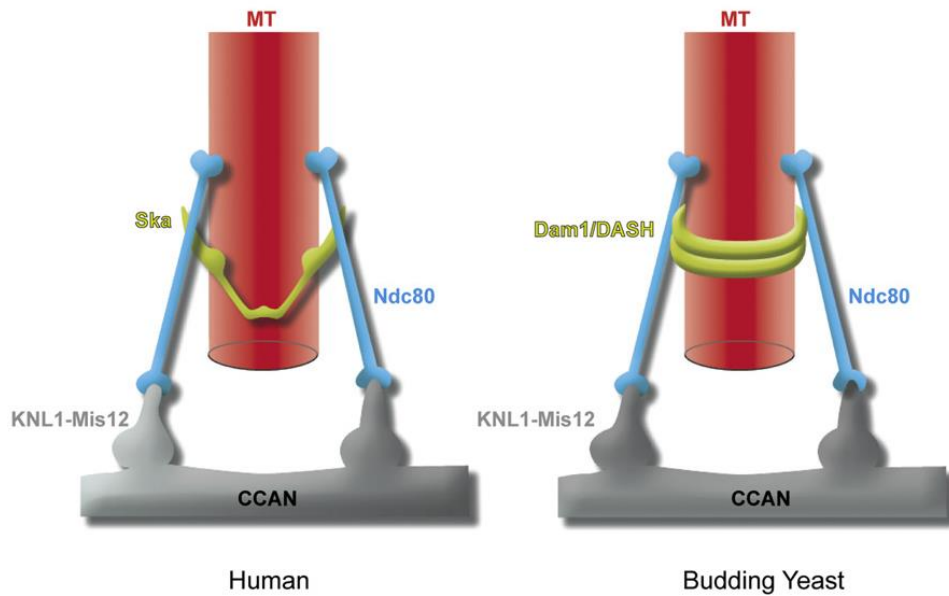


Figure 2.6 This figure summarize the role of Ska and DAM1/DASH complexes in stabilizing kinetochore-microtubule interactions in humans (left) and in *S. Cerevisiae* (right)³⁴.

A very simplified scheme which demonstrates how the KMN network motor proteins interact to each other and transfer the force generated on the unstable plus ends of a MT to chromosome.

2.3.2 Ska complex structure and functions

Ska complex is a homodimer with an extended structure which composed of three components: Ska1, Ska2, Ska3/Rama1. Characterizing the structure of the Ska complex and analyzing its influences on the MT binding in vitro and mitotic progression in vivo might explain the interdependency of the protein subunits of Ska complex and their role in the MT binding during cell division^{34,36–38}. The structural core of Ska complex (Ska1 Δ C-Ska2-Ska3 Δ C) is approved to be more suitable for the structural analysis. This core is constituted by Ska1 (1-91), a complete chain of Ska2 and Ska3 (1-101) with the same oligomeric positions as the full-length complex.

Ska1 Δ C-Ska2-Ska3 Δ C is a truncated form including two perpendicular helical beams developed by three Ska complex units. The smaller beam is composed of N-terminal of Ska1 (amino acids 4-31), Ska2 (aa 1-32) and Ska3 (aa2-30) and it is 4 nm long. The Larger bundle instead is about 9 nm

consisting of Ska1 (aa 33-87), Ska2 (aa46-93) and Ska3 (aa 35-98), the C-terminal of Ska2 (aa102-113) surrounds the long bundle. Ska2 junctions to the structure are more flexible and two bundles are fastening to each other in a rigid way and Ska3 plays a pivotal role here because of hydrophobic interactions (Ala28 and Phe36) and polar interactions (between Glu33 and Arg27, and between Asp35 and Arg24) (Figure 7A)^{34,38,39}.

Where the funnel-like configuration of the short bundle closes, the three helices contribute with hydrophobic bindings. Van der Waals interactions create a great hydrophobic core along the long bundle associated with electrostatic contacts. For example, as demonstrated in (figure 7B and 7C), Ska1 Arg27 interacts with Ska2 Glu29 or Ska1 Gln63 and Ska2 Gln71 are connecting to each other. Development of salt bridges is another interaction observed mostly on the external surfaces such as Ska1 Glu45 to Ska3 Lys 55 and Ska1 Glu57 with Ska2 Arg56 (figure 7D). Ska1 is necessary and is applied as a scaffold for the interactions between Ska2 and Ska3³⁴.

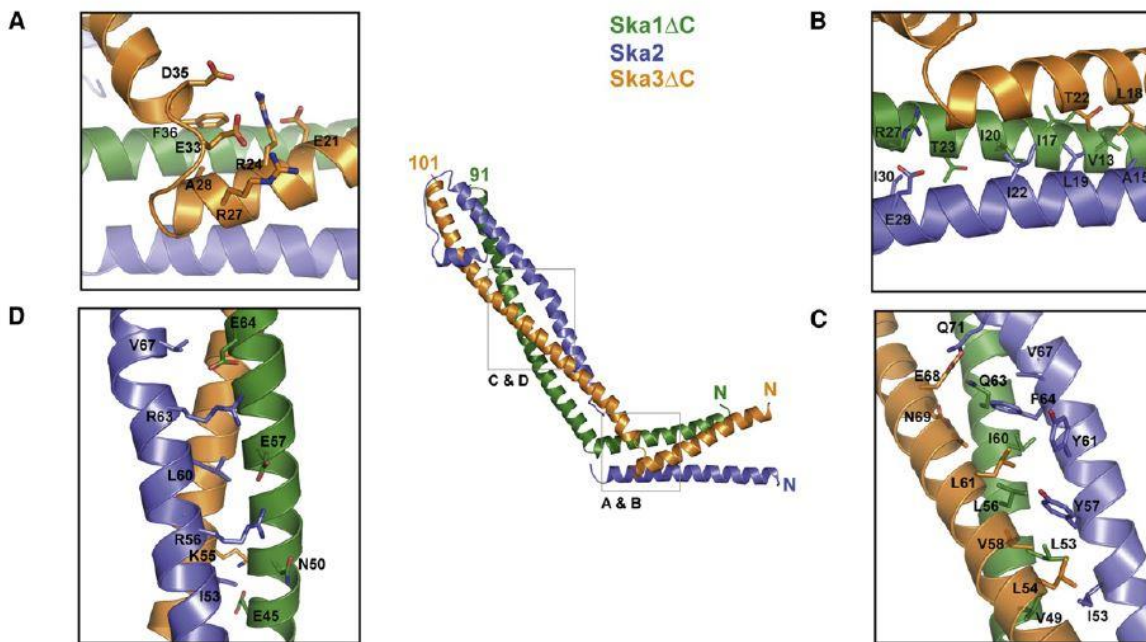


Figure 7. Coiled-coil Structure of the Ska Complex³⁴

W-shaped form is the relevant dimer for Ska1 Δ C-Ska2-Ska3 Δ C molecule and the N-terminal ends of the small bundles encounter to configure dimerization port, while the C-terminal ends of the large bundle face to solvent. This core complex crystal configuration without C-terminals of Ska1 and Ska3 is not sufficient to function *in vivo*^{34,39}.

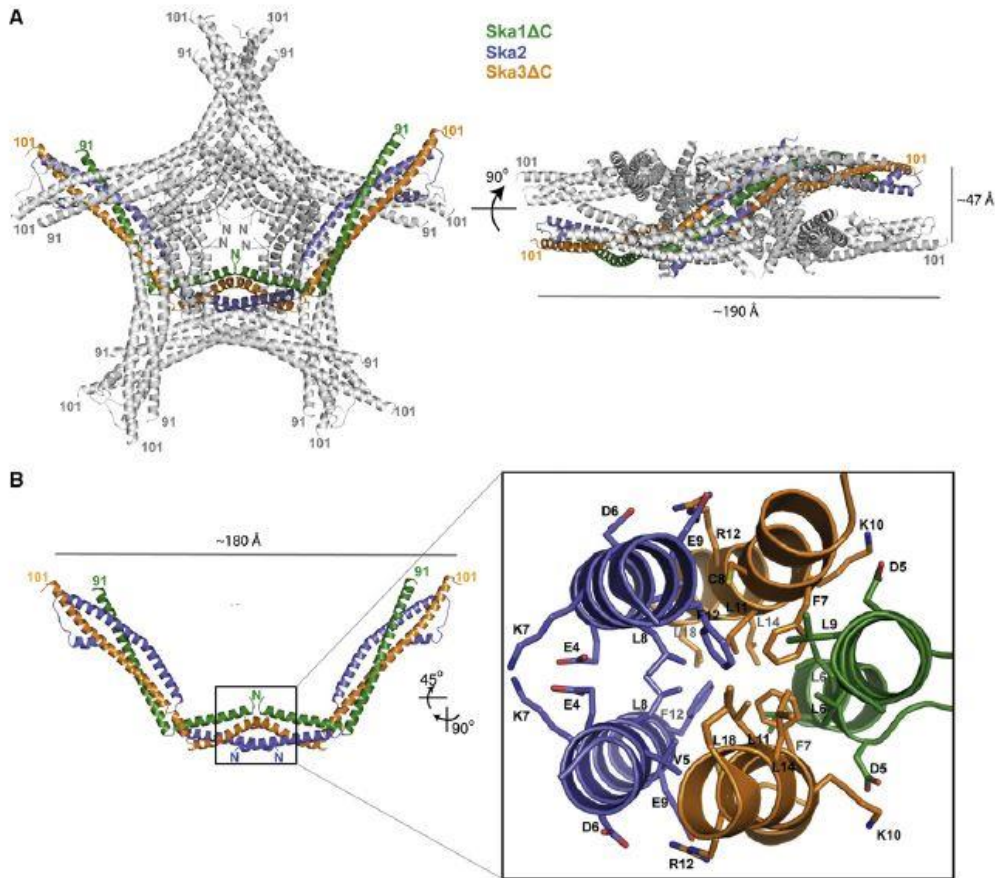


Figure 8 The coiled core homodimer of Ska Complex³⁴

The full length of Ska complex (Ska1-Ska2-Ska3) is 350 Å maximum comparing to 180 Å of Ska1 Δ C-Ska2-Ska3 Δ C (Figure 8). Anyway, *in vivo* the C-terminal domains of Ska1 and Ska3 are necessary³⁴.

2.3.3 Interaction characteristics of Ska complex with microtubules

The MT-binding domains (MTBDs) of the Ska complex have transversal bindings with MTs and these connections are at the ends of W-shaped homodimer. But how the Ska complex interact with microtubules? The answer is achieved by essays uniting X-ray crystallography, cross linking

mass spectrometry (MS) and biochemistry. Ska complex have various orientations to link tubulin heterodimers via its MT contact sites and these binding domains interact with monomers of tubulin³⁴.

Both Ndc80 and Ska complex consist of a central coiled coil core decorated with peripheral domains at either end. Binding to MTs requires the C-terminal acidic tail of tubulin. Acidic tails of tubulin named 'E-hooks' are the recognized fragment of MTs by MT-interacting proteins. For example, these fragments have an important role in Ndc80-MT binding. On the other hand, seems that acidic tails of tubulin do not participate in Ska complex-MT bindings, although Ska complex interact with tubulin in multiple bindings. At least three tubulin binding domains within Ska1-MTBD contribute in MT recognition^{36,39-42}.

Ska complex contains MT binding domains at both ends of coiled coil while Ndc80 has MT binding domains just at one end. The symmetrical microtubule binding of Ska complex is vital in vivo. In the presence of the Ndc80, Ska complex might bridge two different protofilaments distant practically half of the MT circumference. It can reinforce the longitudinal bindings between Ndc80 and protofilaments by transversal interactions^{34,41,43}. Ndc80 complex interact with microtubules by acknowledging the dimeric interface of α and β tubulins, so the interaction will be sensible to the conformational situation of microtubule protofilaments. In fact, Ndc80 binds straight segments of protofilaments other than flared protofilaments. On the contrary, Ska1-MTBD can bind to tubulin monomers therefore Ska complex is able to bind straight and curved protofilaments indiscriminately^{36,38,40,41,43,44}.

2.3.4 Ska-1 microtubule binding domain

W-shaped homodimer of Ska complex binds transversally to MT thanks to the MT-binding domain (MTBD) which stick out of the ends. Ska complex acknowledge the MTs in a conformation free method, therefore it can bind MTs in variant orientations through its MT binding sites³⁶.

The C-terminal domains of Ska1 (92-255) and Ska3 (102-412) are necessary for microtubule bindings. Ska1 (133-255) (called MTBD) is the most efficient fragment of Ska complex, if

dimerized. This fragment accompanied with Ska1 (92-132 referred to as Loop) binding to helical domain of Ska1 (1-91) are needed for mitotic progression. Ska1-MTBD is also required for primary chromosome alignment, mitotic progression and formation of the strong attachments between microtubule and kinetochore. It is about 5nm long and about 3nm wide. Even if Ska1-MTBD is necessary for accurate mitotic progression, but it is not enough, and fails to localize to KTs. This is because of absence of interactions with Ska2 and Ska3 and the loop which precedes it; therefore, N-terminal and loop are also vital for complete functionality of the Ska complex. Ska1-MTBD has an adjusted winged-helix motif famous for its ability to interact with DNA and protein-protein bindings; residues 133-142 precede eight α -helical fragments (α 1- α 8) and a C-terminal β -hairpin³⁵⁻³⁷.

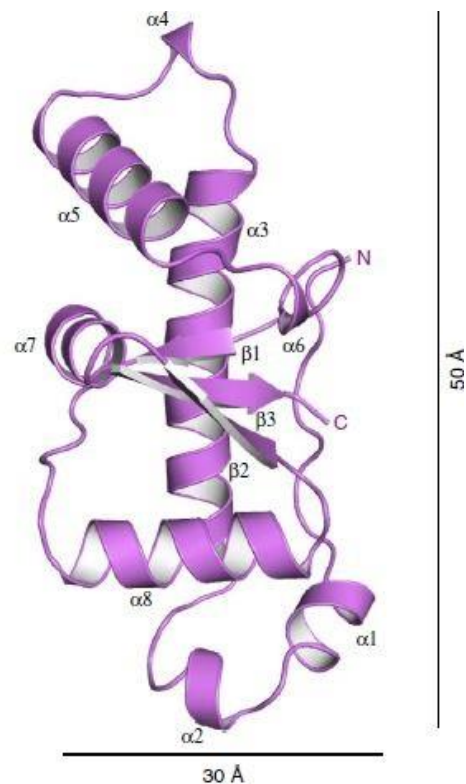


Figure 9 Human Ska1-MTBD³⁶

Incubation of the dynamic microtubules with Ska1 complex demonstrated that Ska1 complex enforces the establishment of the curved microtubules because Ska1 complex can arrange

protofilaments in rings and spiral formation of tubulin dimers. Ska1 complex affiliate directly to the depolymerizing microtubules, so it propagates along depolymerizing microtubules, not only on the straight protofilaments but also the curved structures. Microtubule co-sedimentation assays (a well-established technique in biochemistry) approve a synergy between Ska1 complex and Ndc80 both for human and *C. elegans*. These experiments show that for example human Ndc80 increments the affinity of human Ska1 complex eight times on the microtubule lattice^{35,37,41-43}.

Human Ska complex binds MTs through a multipartite binding mode (multiple MT contact sites). Analysis of the electrostatic surface potential demonstrated that on the surface of the Ska1-MTBD positive charges are present: the hypothesis that Ska complex identify MTs via polar connections take place^{35,36,42}.

2.3.4.1 Ska1-MTBD mutations with Ala to discover active binding sites

Lys/Arg residues that cluster on the surface, were mutated to Ala to acknowledge the crucial residues for MT bindings: these mutations demonstrated notable diminutions in MT binding. The mutation of multiple clusters (K183/184/203/206/217/223/226/227/R236/245A) almost completely abolished MT binding and the multipartite bindings between Ska1MTBD and MTs was confirmed^{36,42}. Figure 10 shows a map of the cross-linked residues between Ska1-MTBD and MTs. Two clusters among the three critical K/R clusters for MT bindings (K183/184/203/206 and K217/223/226/227) demonstrated cross-links with tubulin monomers: these clusters contact globular/folded areas of tubulin monomers. The connections are at two helices: H3 and H4 of β -tubulin and H3 and H12 of α -tubulin. In addition, Ska complex can bind MTs in multiple different orientations: this happens because Lys clusters of Ska1 and the Asp/Glu clusters of tubulin dimers have the possibility to interact in a variety of directions. Therefore, we notice the presence of a multiple fashion of Ska-MT cross-linking. The very interesting contact site between β -tubulin and Ska1-MTBD (Glu110, 156 and 162 in H3) is near the GTP-binding domain and around the zone of lateral contacts between neighboring MT protofilaments^{36,42}.

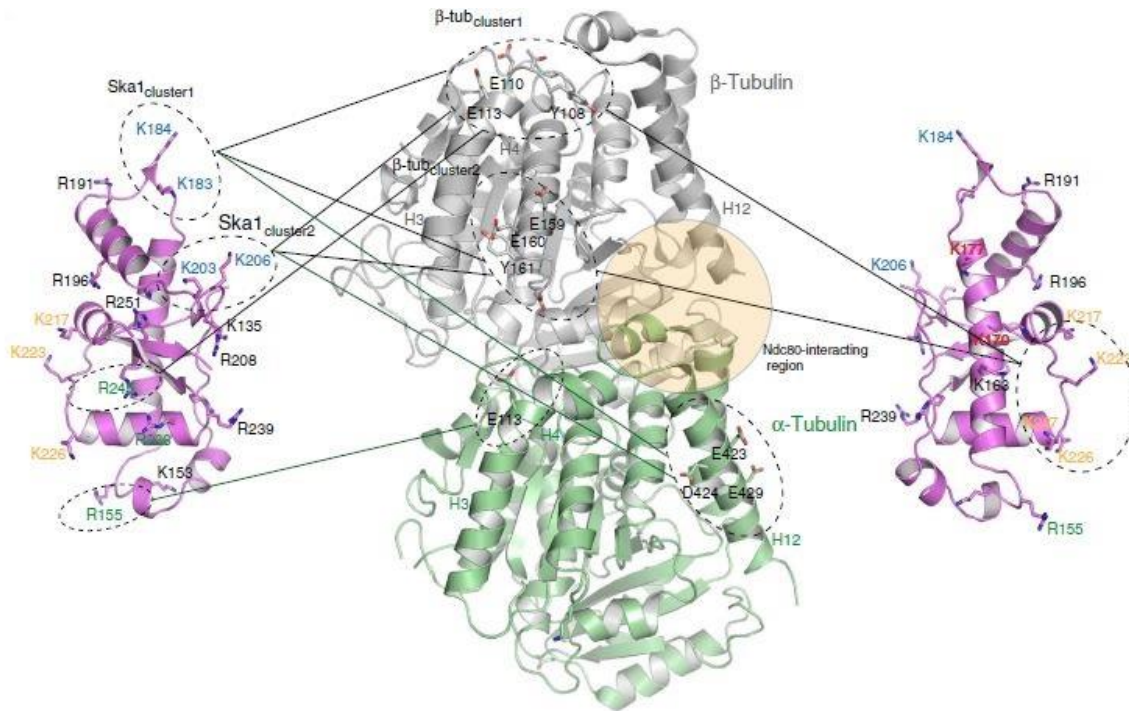


Figure 10 Cross-linking between tubulin dimer and Ska1-MTBD. Cross-links between K/R clusters of Ska1 and Glu/Asp/Tyr/Thr of β -tubulin (grey) and α -tubulin (green). Ndc80 interactions with tubulin (orange)³⁶.

2.4 FORCE GENERATION MECHANISMS IN KINETOCHORE-MICROTUBULE JUNCTIONS

2.4.1 Hydrolysis cycles and polymerization of tubulin

The morphological flexibility of cell derives from non-equilibrium functioning of the cytoskeleton. The energy required for this active state originates from hydrolysis of nucleotides-GTP bound to tubulin⁴.

In the polymerization phase, the addition of subunits containing GTP forms a nucleotide triphosphate (T) cap and speeds up the hydrolysis at internal subunits (Figure 11). Hydrolysis of GTP in the cap turns the filament into a shrinking phase. In this phase GDP containing subunits dissociate. The experimental data confirm this model while declaring that cytoplasmic concentration of GTP is much more than GDP, so the main part of monomers carry a GTP. Biochemical assays demonstrate that joining a tubulin to microtubule increases the GTP

hydrolysis rate to more than 0.2 s^{-1} . Therefore, microtubules older than some seconds have only GDP subunits^{16,45}.

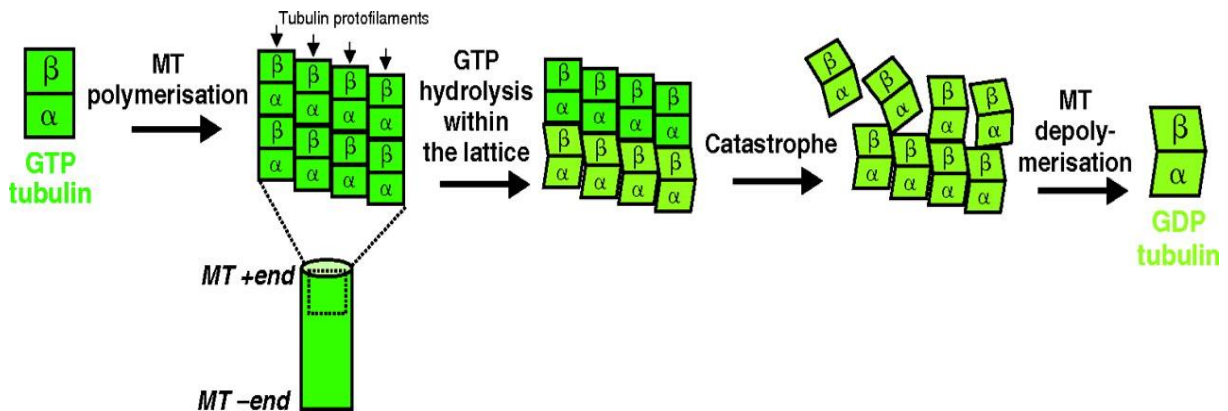


Figure 11. GTP hydrolysis within the lattice⁴⁶.

2.4.2 Force generation by depolymerizing microtubules

In vivo experiments demonstrate that during later stages of mitosis, the spindle formed by microtubules elongates causing the separation of the poles. This happens because microtubules polymerize and create forces greater than 3 pN per microtubule¹⁶. Generation of force by polymerization and depolymerization is inferred also via experiments in vitro. These in vivo and in vitro experiments confirm the force generation in cell even without interference of the motor proteins^{16,23,24,47,48}.

But how much great are these forces?

The force generated by an actual polymer does not surpass the equilibrium force which is completely independent of the polymerization mechanism. It is established both for a direct contact with a particle and the contact by means of accessory proteins (the kinetochore, in case of microtubules).

The equilibrium force for a monomer concentration $[A_1]$ with no net polymerization is:

$$F_{eq} = \frac{kT}{\delta} \cdot \ln\left(\frac{[A_1]}{K_c}\right) \quad (2.1)$$

K_c is the critical concentration if no external force is implicated and δ is the increment of the length when added a monomer, kT is Boltzmann coefficient multiplied by temperature.

It is not easy to imagine how a growing or shrinking filament might push or pull on a particle. It is might be taught that the particle probably impedes the polymerization and in the case of depolymerizing polymer it is difficult to conceive how a shrinking filament remain in contact with the particle. Declaring these issues, another question also emerges: is the polymerization process rapid enough?

The Brownian ratchet model is one of the solutions for this question (Figure 3), which considers a filament composed of n monomers, with one termination anchored and the other confined the particle. It is presumed that the particle can diffuse and the distance or gap (x) between the ultimate monomer and particle surface changes. The gap might be “open” or not: an open gap means that x exceeds δ , so increases the probability of binding a monomer to form a $(n+1)$ -mer. Alternatively, a monomer could unbind to create a $(n-1)$ -mer.

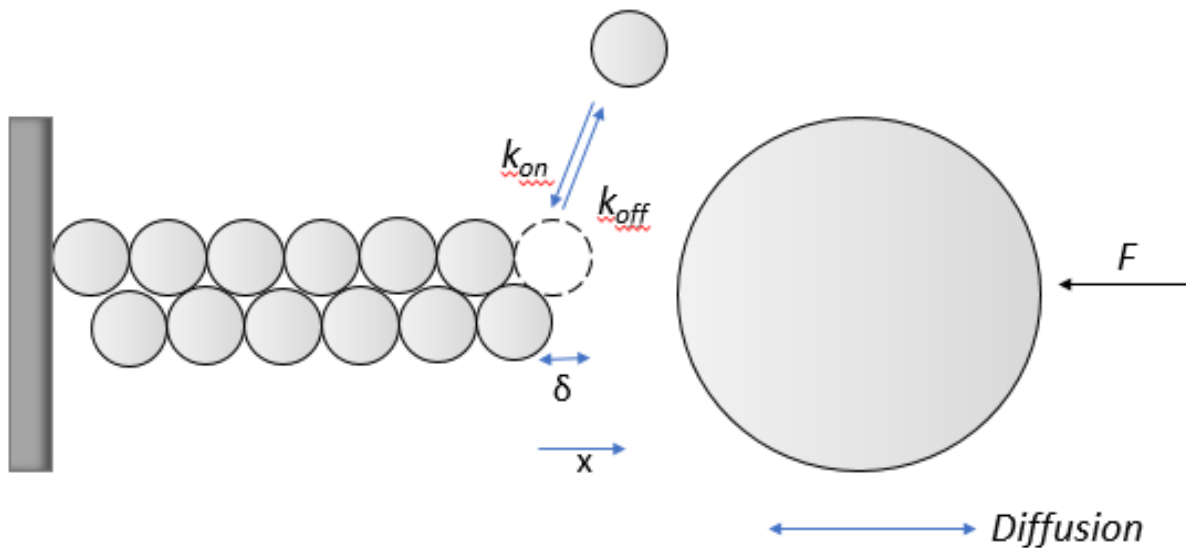


Figure 12. The Brownian ratchet mechanism demonstrating the force generation by polymerization

This process can be *reaction limited* or *diffusion limited*. In the case of reaction limited, diffusion is very fast and very occasionally a monomer bind. The elongation rate is:

$$v = \delta \frac{dn_{av}}{dt} = \delta(k_{on}[A_1]e^{\frac{-F\delta}{kT}} - k_{off}) \quad (2.2)$$

where k_{on} and k_{off} are association and dissociation rate constants, n_{av} is the average length of the filament, $[A_1]$ is the monomer concentration, δ is the increment of the length when added a monomer and kT is Boltzmann coefficient multiplied by temperature.

At equilibrium $K_c = k_{off}/k_{on}$ so the equation above reduced to the equilibrium equation.

In the contrary in case of diffusion limited polymerization the monomer drops in the gap more probably, immediately after opening a gap and the elongation rate is calculated:

$$v = \delta \frac{dn_{av}}{dt} \cong \frac{2D}{\delta} \left[\frac{(F\delta/kT)^2/2}{e^{F\delta/kT} - 1 - F\delta/kT} \right] \quad (2.3)$$

where D is the diffusion coefficient of the particle, n_{av} is the average length of the filament, $[A_1]$ is the monomer concentration, δ is the increment of the length when added a monomer and kT is Boltzmann coefficient multiplied by temperature¹⁶.

2.4.3 Force Generation within the Microtubule Lattice

Through the mechanism, furnished by hydrolysis, a high quantity of mechanical energy accumulates in the microtubule lattice. While the GDP-tubulin has a more strained configuration which avoid it to place well in the microtubule lattice, then it has a much higher critical concentration respect to GTP-tubulin. When association and dissociation are in equilibrium, force will be maximum:

$$F = \frac{kT}{\delta} \ln \left(\frac{k_{on}^T [A^T] + k_{on}^D [A^D]}{k_{off}^T p^T + k_{off}^D p^D} \right) \quad (2.4)$$

$[A^T]$ and $[A^D]$ are cytoplasmic concentration of GTP-tubulin and GDP-tubulin, p^T and p^D are the proportion of GTP- and GDP-subunits in the cap, k_{on}^T and k_{on}^D are association rates of GTP- and GDP-dimers, k_{off}^T and k_{off}^D are dissociation rates of GTP- and GDP-dimers

Over fast polymerization cycles, maximum proportion of GTP-tubulin at the cap ($p^T=1, p^D=0$) and the microtubule imposes a maximum compression force as follows:

$$F_{polym} \cong \frac{kT}{\delta} \ln\left(\frac{k_{on}^T[A^T]}{k_{off}^T}\right) = \frac{kT}{\delta} \ln\left(\frac{[A^T]}{K_c^T}\right) \quad (2.5)$$

where K_c^T is the critical concentration of GTP-tubulin.

On the contrary during rapid shrinkage there is no GTP in cap ($p^T=0, p^D=1$); so, the maximum force is:

$$F_{depolym} \cong \frac{kT}{\delta} \ln\left(\frac{k_{on}^D[A^T]}{k_{off}^D}\right) \cong \frac{kT}{\delta} \ln\left(\frac{[A^T]}{K_c^D}\right) \quad (2.6)$$

where, K_c^D is the critical concentration of GDP-tubulin ^{16,48}.

3. METHODS

3.1 Computational molecular modeling

Computational molecular modeling is a theoretical method able to describe complex biochemical systems such as proteins in terms of a realistic atomistic description aimed at calculating macroscopic physical properties of these systems. Macroscopic physical properties can be distinguished in static equilibrium properties (e.g., potential energy, potential of mean force, radial distribution function) and dynamic or non-equilibrium properties: (e.g., viscosity, diffusion processes). Macroscopic properties can be considered as ensemble properties, i.e. averages over a representative statistical ensemble, which defines all the physical states of a molecular system. In order to calculate these properties, not only the knowledge of a single structure is required, but also the generation of a representative ensemble at a given temperature is necessary. These two requirements are not enough when thermodynamic equilibrium properties based on free energies (e.g., binding constant, solubility, relative stability of molecular conformation, etc.) have to be calculated. The computation of free energies and thermodynamic potentials requires specific molecular simulation techniques.

For the generation of a representative equilibrium ensemble two methods are available: Monte Carlo simulations and Molecular Dynamics (MD) simulations. For the generation of non-equilibrium ensembles and for the analysis of dynamic events, only MD is the suitable tool.

MD simulations have been widely used in the last three decades aimed at obtaining new insights in biological functions of protein by studying such molecular systems at atomistic level. Conformational changes have been computationally analysed by atomistic simulations, since McCammon et al. ⁴⁹ studied the dynamic behavior of small protein based on MD simulation. Moreover, the thermal fluctuation behavior of small proteins has been well understood by the sampling the trajectories obtained from MD simulations ⁵⁰. Other studies have been conducted by Lu et al., who investigated the mechanical unfolding of a protein, such as titin, via MD simulations applying a mechanical loading to the terminals of a protein (Steered MD simulations)^{51,52}. Reading over these successes, it is noticeable that the accessible time scale for

molecular dynamics¹ is in the order of hundred nanoseconds⁵³, whereas proteins perform their functions at much larger time scale ranging from at least nano-seconds to a few seconds. Even though atomistic simulations have permitted to investigate protein dynamics utilizing energy functions or parameters specific for the atoms of the system, the mechanics of large protein structure is computationally inaccessible with molecular dynamic simulations. The computational difficulty in MD lies in the computation of the force that requires the calculation of the gradient of a non-harmonic potential field. Also, the size of the system in terms of amount of atoms is a strong limitation for long time simulations, considering that the environment surrounding the protein is usually water, explicitly modeled (e.g., SPC). For example, in the case of cytoskeleton proteins, which are globular and large (around 800 residues) as tubulins or actins, the simulated system (e.g., a clusters of these proteins) could easily be composed of about 200,000 or even 500,000 atoms. Even if nowadays extensive clusters of thousands of CPU can be used to run MD simulations in parallel, there are anyway software limitations that restrict the speeding up of CPUs working in parallel. This indicates that MD simulations may be computationally inhibited for the analysis of very large protein mechanics, where higher spatial and temporal scales are required.

¹ The time step for integrating the equation of motion is typically in the order of 10^{-15} seconds (fs).

3.2 Molecular Dynamics

MD is an important tool for understanding molecular processes at atomic level, and due to the computational power, which has become available over the last decade, both MD relevance and usage are rapidly growing.

MD simulations solve the Newton's equations (eq. 3.1) of motion for a system constituted by N interacting atoms with position r_i and mass m_i :

$$m_i \frac{d^2 r_i}{dt^2} = F_i, i = 1 \dots N, \quad (3.1)$$

where the forces F_i acting on the i^{th} -atom are the negative derivatives (eq. 3.2) of the potential energy function $V(r^N)$:

$$F_i = -\nabla V. \quad (3.2)$$

The equations of motion are solved by integrations in small time steps (usually fs), thus during the simulation at every time step, the position and the velocity of every single atom in the system are known. After initial changes the molecular system usually reaches an equilibrium state. By averaging data over the equilibrium trajectories, many macroscopic thermodynamic properties can be calculated (Figure 3.1).

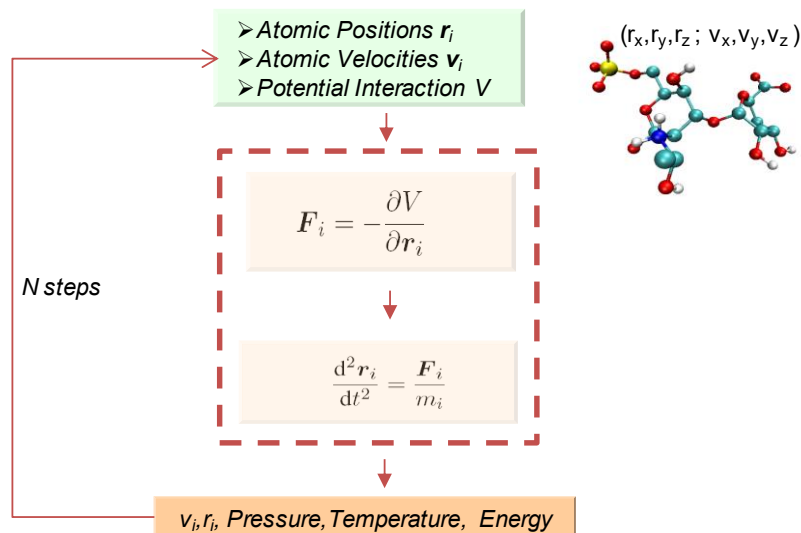


Figure 3.1 MD algorithm scheme: the initial positions and velocities are provided as input data. Based on the positions, r_i , and the potential energy, V (which describes the interactions between particles as a

function of their distance), the forces, \mathbf{F}_i , on each particle are calculated. Integration of the equation of motion allows the calculation of new velocities, \mathbf{v}_i , and positions, \mathbf{r}_i . The cycle continues for as many time steps as the simulation lasts. Macroscopic thermodynamic properties (e.g., pressure, temperature, energy) can be calculated as ensemble averages.

Each step needs initial position and velocity of all the atoms in the molecular system as input data, while the forces are calculated by the potential energy. At the first iteration, if the velocities are not defined they can be assigned as the atom velocities for a system at a defined temperature, for example 300 K, following a Maxwell-Boltzmann distribution.

Usually, the starting configuration of the molecular system is very far from the equilibrium requiring energy minimization phases before running a MD simulation due to the presence of excessively large interaction forces among the atoms.

Employing Newton's equation implies the use of classical mechanics to describe the atoms' motion. This is correct for most heavy atoms at normal temperatures (e.g., carbon), but there are exceptions which cannot be properly treated by MD, in particular quantum phenomena or events characterized by very high vibration frequencies, let's say higher than 100 cm^{-1} . This means that for example all bond and bond-angle vibrations cannot be properly calculated by MD. In order to overcome this problem, bonds (and bond angles) are usually constrained, by means of specific algorithms as LINCS⁵⁴, in the equation of motion. Moreover, MD approach uses conservative force fields, which are function of the atomic positions only. This implies that the electronic motions are not considered but rather, as the Born-Oppenheimer approximation states, electrons are supposed to adjust their dynamics instantly following the atomic position.

A force field is just a set of parameters which specify the functional expressions describing interactions among atoms. This set of parameters is usually derived empirically or by means of quantistic approach, and for this reason MD belongs to the category of the empirical molecular modeling methods. The force field parameters take into account all the static properties of the system, such as the covalent bond constants, while the atom positions or velocities describe the dynamics of the system. In particular the force field parameters represent the constants of the

functional expressions describing all bond and non-bond interactions among atoms.

3.2.1 The potential energy function

Atom interactions are taken into account in terms of potential energies. The potential energy is a multidimensional function (eq. 3.3) of the coordinates, r_i , of all the N particles in the system. The potential energy function can be split in two main terms:

$$V(r^N) = \{E_B(r^N)\} + \{E_{NB}(r^N)\}, \quad (3.3)$$

where E_B is the sum of all the functional expressions describing the bond interactions among the atoms in the system and E_{NB} is the sum of the functional expressions describing the non-bond interactions in terms of van der Waals and electrostatic contributions.

An example of potential energy function is reported in eq. 3.4:

$$V(r^N) = \left\{ \frac{1}{2} k_{ij} (r_{ij} - r_{0,ij})^2 + \frac{1}{2} \xi_{ijk} (\cos(\theta_{ijk}) - \cos(\theta_{0,ijk}))^2 + \psi_{ijkl} (1 + \cos(n\varphi_{ijkl} - \varphi_{0,ijkl})) \right\} \\ + \left\{ 4\epsilon_{ij} \left[\left(\frac{\sigma_{ij}}{r_{ij}} \right)^{12} - \left(\frac{\sigma_{ij}}{r_{ij}} \right)^6 \right] + \frac{q_i q_j}{4\pi\epsilon_0 \epsilon_r r_0} \right\} \quad (3.4)$$

The first three terms in the sum (eq. 3.4) represent the bond interactions (Fig. 3.2a) while the last two terms represent the non-bond interactions.

The covalent bond interaction is defined by:

$$E_{bond} = \frac{1}{2} k_{ij} (r_{ij} - r_{0,ij})^2 \quad (3.5)$$

The two constants (eq. 3.5) represent the bond stiffness, k_{ij} , and the equilibrium distance $r_{0,ij}$, and depend on the type of particles being bonded together.

The angle bond contribution (Fig. 3.2b) includes any interaction between three atoms, i , j , and k , bound together covalently; the potential energy (eq. 3.6) is expressed as function of the angle, ϑ_{ijk} , formed by the three atoms, the equilibrium angle, $\vartheta_{0,ijk}$, and the stiffness, ξ_{ijk} , of the angle bond:

$$E_{angle} = \frac{1}{2} \xi_{ijk} (\cos(\theta_{ijk}) - \cos(\theta_{0,ijk}))^2 \quad (3.6)$$

The dihedral bond interactions (Fig 3.2c), also called the proper dihedral interactions, involve four atoms, i, j, k , and l , bound covalently together one after the other.

$$E_{dihedral} = \psi_{ijkl}(1 + \cos(n\phi_{ijkl} - \phi_{0,ijkl})) \quad (3.7)$$

The potential energy (eq. 3.7) is described as function of the stiffness of the dihedral angle, ψ_{ijkl} , the dihedral angle, ϕ_{ijkl} , between vectors normal to the planes spanned by atoms i, j , and l , and atoms j, k , and l , respectively, and the equilibrium dihedral angle, $\phi_{0,ijkl}$.

Given that dihedral interactions may have more than one energy minimum (e.g., *cis* and *trans* configurations), the parameter n imposes a number of minima regularly distributed between 0 and 360°.

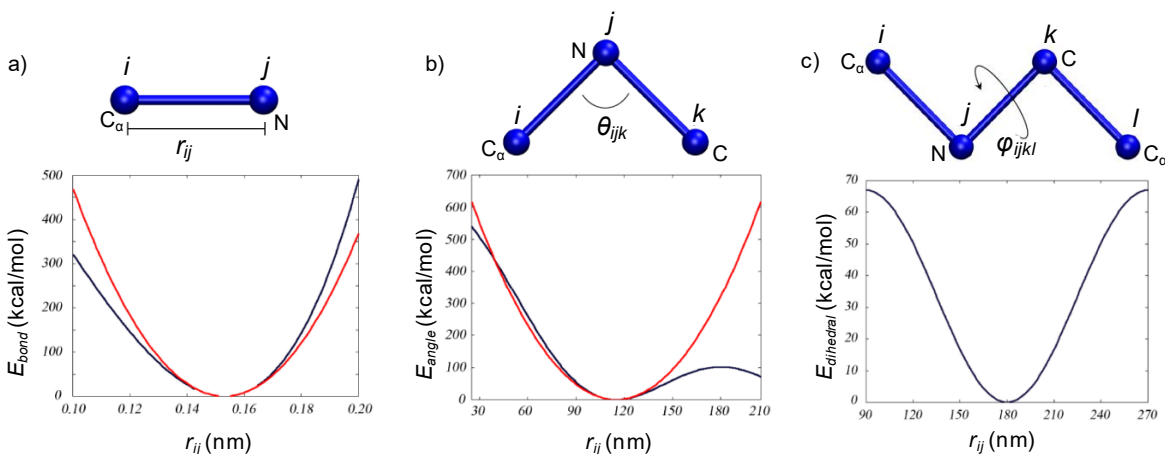


Figure 3.2 a) Bond interaction between 2 atoms, C_α - N , in the protein backbone as function of the atom distance (black curve). A harmonic potential (red curve) with matching coefficients [GROMACS user manual, 2005] is shown for comparison. Referring to eq. 3.5, the constant $r_{0,ij}=0.1530$ nm and $k_{ij}=7.15 \cdot 10^6$ kJ mol⁻¹ nm⁻⁴. b) The angle potential energy as function of the C_α - N - C angle in the protein backbone (black curve), θ_{ijk} , fitted by a harmonic potential (red curve) is shown. Referring to eq.2.6 the constant values are: $\theta_{0,ijk}=115^\circ$, $\xi_{ijk}=6 \cdot 10^{10}$ kJ mol⁻¹. c) The dihedral potential energy as function of the angle in degrees for the protein backbone (black curve) consisting of C_α - N - C - C_α is shown. The energy minimum when the angle is 180° corresponds to a *cis* configuration.

The latest two terms in eq. 3.4 are the non-bond interactions: van der Waals and Coulomb energies. The Coulomb energy, $E_{Coulomb}$, takes into account the electrostatic interactions between

charged particles and the Lennard-Jones energy, $E_{Lennard-Jones}$, accounts for a combination of excluded volume effects and van der Waals interactions.

Coulomb interactions exist between any two (partially) charged particles, i and j , and depend on their charges, q_i and q_j , and the distance, r_{ij} , between them as:

$$E_{Coulomb} = \frac{q_i q_j}{4\pi\epsilon_0\epsilon_r r_0}. \quad (3.8)$$

The factor $(4\pi\epsilon_0\epsilon_r)^{-1}$ is the electric conversion factor equal to $138.9 \text{ kJ mol}^{-1} \text{ nm e}^{-2}$, where ϵ_0 is the so called free space permittivity and ϵ_r is the relative permittivity. The energy depends on the distance between the two particles as r^{-1} : thus the electrostatic energy is a long-range interaction.

The Lennard-Jones energy describes two kinds of forces working on two different distances:

$$E_{Lennard-Jones} = 4\epsilon_{ij} \left[\left(\frac{\sigma_{ij}}{r_{ij}} \right)^{12} - \left(\frac{\sigma_{ij}}{r_{ij}} \right)^6 \right]. \quad (3.9)$$

The first term (eq. 3.9) describes the very short-range repulsion due to electron orbitals, which begin to overlap, whereas the second term describes a long-range van der Waals attraction energy. The two parameters, σ_{ij} and ϵ_{ij} , are atom dependent and provide the shortest distance for which the Lennard-Jones energy is zero and the depth of the potential well, respectively (Fig. 3.3).

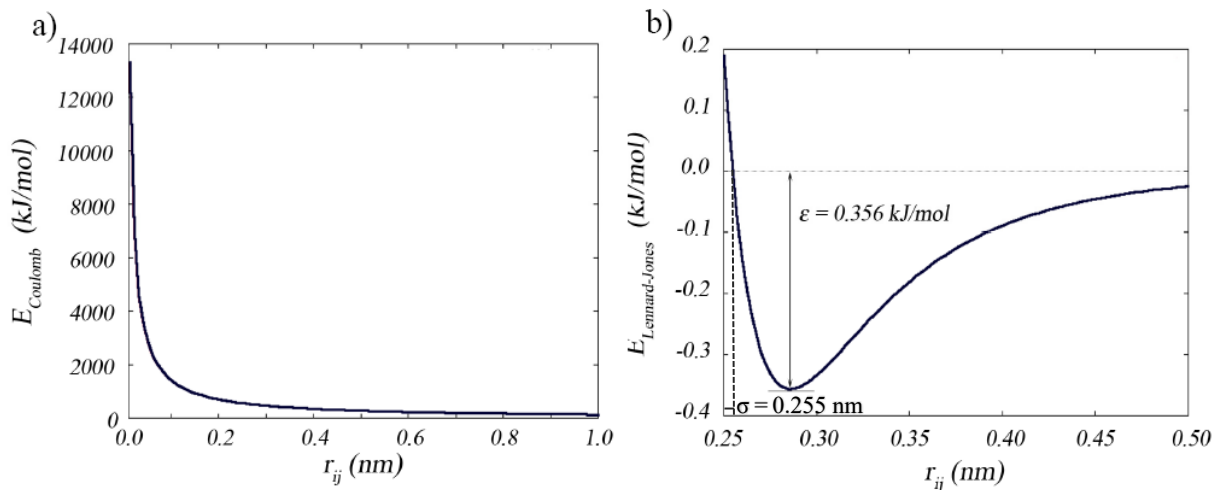


Figure 3.3 (a) The Coulomb energy as function of the distance, r_{ij} , between two particles with the same charge ($1e$). Notice that the atoms inside a protein are hardly ever fully charged, instead they are either uncharged or partial charged. (b) The Lennard Jones energy as function of the distance. The energy corresponds to the interaction between a Mg^{2+} -ion and a C-atom (not C_α -atom) in the backbone of a protein. The shortest distance for which the Lennard-Jones energy is zero, σ , and the depth of the potential well, ϵ , are equal to 0.255 nm and 0.356 kJ mol^{-1} , respectively.

3.2.2 Periodic boundary conditions

Before starting a MD simulation the molecular system is inserted in a space-filling box and usually surrounded by water (implicitly or explicitly modeled). When such finite system has to be simulated, the classical way to minimize edge effects is to apply periodic boundary conditions. All the atoms in the box are surrounded by translated copies of the box making the system without boundaries. In this way the artifacts caused by false boundaries in an isolated cluster are now replaced by the artifacts due to applied periodic conditions (Fig. 3.4). If a crystal or a periodic system is simulated, such periodic boundary conditions are needed.

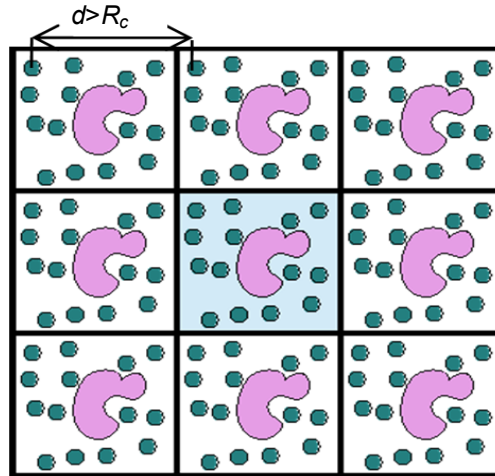


Figure 3.4 Periodic boundary conditions: the central molecular system is replicated in copies creating an infinite system. The cutoff distance (R_c) should be less than the size of the box (d) in order to avoid an atoms seeing their replicas.

In the case of non-periodic systems, as liquids or solutions, the periodicity by itself causes errors, but such errors are expected to be less severe than the errors resulting from the modeling of a non-natural boundary as it happens in vacuum simulations [GROMACS 4.0 user manual, 2005].

3.2.3 Treatment of the non-bond interactions

The most time-consuming part of a MD simulation is the calculation of the non-bond forces. The number of the non-bond interactions increases as the square of the number of atoms in the system (N^2). There are several ways to deal with such interactions, as an example using the cutoff distance and the minimum image convention.

The minimum image convention states that each atom should see at least an image of every atom in the system if periodic boundary conditions are settled on.

Applying a cutoff distance means that every interaction energy between two atoms is zero if the two atoms are further apart than the cutoff distance. The cutoff is usually not a problem for short range interactions as the Lennard-Jones potentials, which fall off very rapidly⁵⁵. In the case of long-range interactions, the cutoff method is not usually recommended because it causes errors

and strong discontinuities in the potential energy calculations⁵⁵. In particular, the non-bond electrostatic interaction energy between two O atoms of two water molecules as function of their distance is shown in Fig 3.5. Imposing a cutoff distance equal to 8 Å, high distortions in the energy profile are observed.

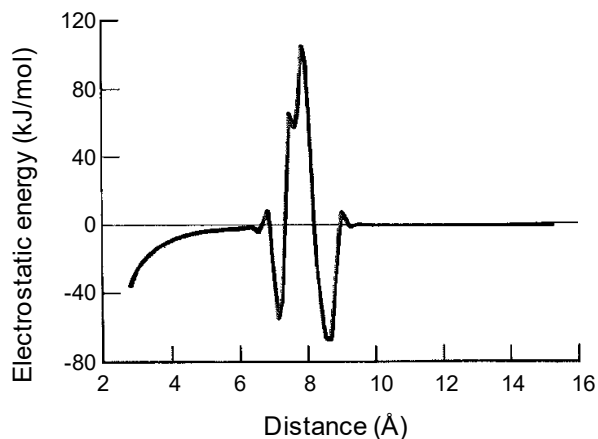


Figure 3.5 High variations in the interaction energy of the water dimer as function of the O-O distance, when a cutoff distance equal to 8 Å is applied⁵⁵.

Beyond the cutoff distance there are other methods to avoid such kind of discontinuities: e.g., using a shift function (i.e. add a function to the potential), or using a switch functions (i.e. multiplies the potential with a function⁵⁵). There is no fundamental difference between a switch function and a shift function. Although using these functions reduces the discontinuities in energy calculations, such functions produce a considerable modification of the Coulomb potential. Hence, the effect of such modifications must be carefully evaluated in long-range interactions, where the modifications of the Lennard-Jones dispersion and repulsion are generally minor.

The most correct method to accurately include all the effects of the long-range forces in a computer simulation is called the Ewald summation⁵⁶. The Ewald summation is a method for computing the interaction energies of periodic systems (e.g., crystals). In this method the charge-charge contribution to the potential energy due to all the pairs of atoms, is divided in two summations: the first one is over all the atom pairs interacting in the short range and the second

one is over all the atoms pairs interacting in the long range. Then the first sum is calculated in the real space, while the other one in the Fourier space. The advantage of this approach is the rapid convergence of the Fourier space summation, compared to its real space equivalent, when the real space interactions are in the long range. Thus, a short cutoff distance (in the order of 1 nm) in the direct space sum and a short cutoff distance in the reciprocal space sum (e.g., 10 wave vectors for each direction) can be applied. Unfortunately, the computational cost of the reciprocal part of the sum (Fourier space) increases as N^2 and its application is therefore not realistic for large systems. To overcome this limitation the Particle-mesh Ewald (PME) method was proposed⁵⁷ in order to improve the performances of the reciprocal sum method. Briefly, the Ewald summation method is modified so that the Fast Fourier Transform can be used to calculate the reciprocal space summation. The PME algorithm scales as $N\log(N)$, where N is the number of interacting atoms, and it is considerably faster than ordinary Ewald summation in case of medium or large systems.

3.2.4 Simulated ensembles in molecular dynamics

By proper modification of the equations of motion, several ensembles can be generated.

By keeping Energy (E), Temperature (T) or Pressure (P) constant and considering V as the box volume, N as the number of particles in the system and μ as the chemical potential, five ensembles can be generated: the constant NVE or microcanonical ensemble, the constant NVT or canonical ensemble, the constant NPT or isothermal-isobaric ensemble and the constant μVT or grand canonical ensemble, and finally the constant μPT ensemble.

When MD is performed using just Newton's equations of motion, the total energy is conserved resulting in a microcanonical ensemble. In order to obtain a different ensemble, the equations of motion needs to be modified.

For example in order to obtain a canonical ensemble, the system can be coupled to an external bath at temperature, T , also called the Berendsen thermostat⁵⁰. The weak coupling is achieved with a first order differential equation for the temperature. This causes any deviation from the

reference temperature to decay exponentially (eq. 3.10) following a relaxation constant τ :

$$\frac{dT}{dt} = \frac{(T-T_0)}{\tau}. \quad (3.10)$$

The main disadvantage of the Berendsen thermostat is that the ensemble is actually unknown.

For this reason another approach can be used, the Nosé-Hoover thermostat [Nosé, 1984; Hoover, 1985]. The Hamiltonian of the system is extended by introducing a thermal reservoir and a friction term in the equations of motion. The friction force is proportional to the product of each particle's velocity and a friction parameter, γ as:

$$\frac{d^2r_i}{dt^2} = \frac{F_i}{m_i} - \gamma \frac{dr_i}{dt}. \quad (3.11)$$

This friction parameter can be considered as a dynamic quantity with its own equation of motion (eq. 3.12), where the time derivative is calculated from the difference between the current kinetic energy and the reference temperature:

$$\frac{d\gamma}{dt} = \frac{1}{Q}(T - T_0). \quad (3.12)$$

The reference temperature is T_0 , while T is the current instantaneous temperature of the system. The strength of the coupling is determined by the constant Q , called the *mass parameter* of the reservoir, in combination with the reference temperature.

In this case, even if a canonical ensemble is obtained, the temperature oscillates around the average, where the period of the oscillations depends on the effective mass, Q , associated with the temperature usually resulting in unwanted kinetic effects [Gromacs 4.0 user manual, 2005].

In summary, using weak coupling (e.g., Berendsen) a strongly damped exponential relaxation is obtained, where the fast kinetics are unaffected but the ensemble is unknown, while the Nosé-Hoover approach produces an oscillatory relaxation, where the ensemble is known but unwanted kinetic effects can affect the simulation.

3.2.5 Steered Molecular Dynamics

Steered Molecular Dynamics (SMD) is one of the methods for Enhancing the Conformational Sampling which are developed to overcome the limitations of molecular dynamics both regarding high computational costs and rough energy landscapes. The concept is to implement the more efficient sampling of the conformations in the phase space, trying to overcome energy barriers and spending less resources.

SMD drives the conformations to be sampled in special directions by applying external forces. The system may drive from one microstate to another under application of a bias potential along one or more reaction coordinates. The target is to make observable those processes which are not fast enough for the classical molecular dynamics with the nanosecond time scale limitation.

The Steered Molecular Dynamics simulation puts a constraint on the system, chooses a prescribed path (reaction path) along which microstates could be sampled in the configuration phase space and applies external steering forces, to accelerate above mentioned slow processes.

The critical point is to guarantee that reaction coordinate closely follows the constraint positions. Stiff-spring approximation theory asserts it by choosing the external constant force (F) sufficiently high:

$$F(t) = 2k(vt - x(t)) \quad (3.13)$$

where k is the spring constant of the constraint, v is the pulling velocity and $x(t)$ is the coordinate of the molecule at time t .

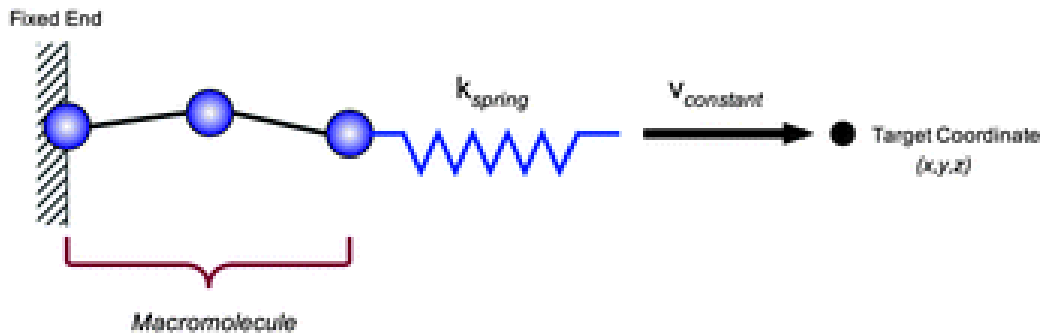


Figure 2. 6 Macromolecule is stretched by a harmonic spring with stiffness of K_{spring} and a constant velocity $v_{constant}$ toward a target coordinate (x,y,z) ⁵⁸

$$W(x(t)) = \int_0^{x(t)} F(t) dx(t) \quad (3.14)$$

The force is integrated over the pulled trajectory for work calculation.

In Figure 14 an example of SMD on an helix structure is represented: the applied force unfolds the secondary structure.

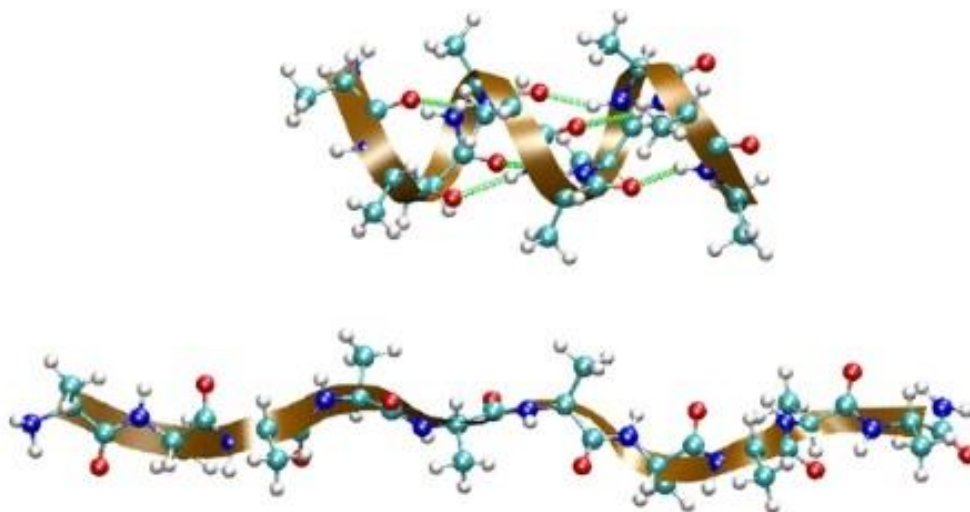


Figure 3.7 Example of a trajectory snapshots from a *Steering* MD of DecaAlanine peptide ⁵⁹.

The Potential mean force (i.e., a cut of the free energy landscape along a defined reaction coordinate, such as the protein length) is determined by Boltzmann-weighted average over all degrees of freedom except the reaction coordinate: these averages determine an approximation of the motion along the reaction coordinate as a diffusive motion on the functional PMF ⁵⁹.

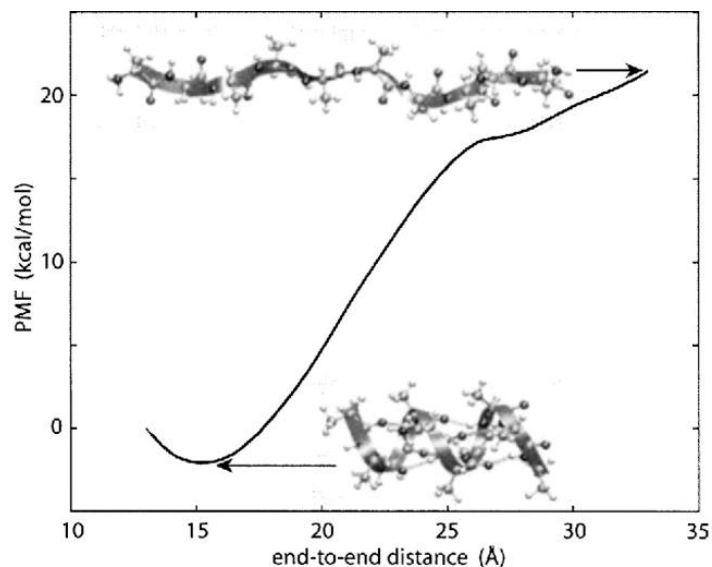


Figure 3. 8. Potential mean force is the free energy profile through the reaction coordinate⁵⁹.

Potential mean force is an equilibrium property; the obstacle is calculating an equilibrium property during a non-equilibrium process as SMD. The work implemented over a non-equilibrium procedure associates to free energy differences by Jarzynski's equality. The work performed on a finite classical system which can exchange energy with a heat reservoir, depends on the external factors during time. If the external parameters vary infinitely slowly along a specific path (e.g. reaction path) the executed total work on the system is the Helmholtz free energy difference ΔG between the initial and final configurations:

$$W = \Delta G = G^B - G^A \quad (3.15)$$

where $G^{A;B}$ are the equilibrium free energy of the system, with the parameters maintained constant at A or B .

Dissipated work associated to the entropy growth because of the irreversibility of the process (the pulling simulation is a typical non-equilibrium simulation) is:

$$W_{diff} = \bar{W} - \Delta G \quad (3.16)$$

where \bar{W} is the average of an ensemble of W measurements obtained by several simulations carried out with different initial conditions (e.g., initial velocities, initial configuration).

The Jarzynski's equality assessed the possibility to obtain equilibrium information ΔG from the ensemble on non-equilibrium (finite time) measurements.

$$e^{-\beta\bar{W}} = e^{-\beta\Delta G} \quad , \quad \Delta G = \frac{1}{\beta} \ln(e^{-\beta\bar{W}}) \quad (3.17)$$

Where $\beta = 1/k_bT$. This result, which is independent of both the path from A to B, and the rate at which the parameters are switched along the path, is surprising: it says that we can extract an equilibrium properties, i.e., the free energy ΔG , from the ensemble of non-equilibrium (finite-time) measurements described above^{60,61}

3.3.4 Software packages

There is a wide variety of MD codes for biomolecular simulation: AMBER, CHARMM, GROMACS, NAMD, etc. GROMACS (GRONingen MACHine for Chemical Simulations) is a molecular dynamics simulation package originally developed in the University of Groningen, now maintained and extended at different places and university. GROMACS is written for Unix-like operating systems and the entire package is available under the GNU General Public License. GROMACS is a versatile tool to perform molecular dynamics simulations and energy minimization. It is primarily designed for biochemical molecules like proteins, lipids and nucleic acids that have a lot of bonded interactions, but it is very fast in the calculation of non-bonded interactions, and for this reason many research groups are also using it for non-biological systems, e.g. polymers⁶².

4. TUBULIN-SKA INTERACTION CHARACTERIZATION BY MOLECULAR MODELLING WITH ATMOIC RESOLUTION

4.1 INTRODUCTION

Microtubules (MTs) are the key components of the cell which perform a fundamental duty in the cellular processes, especially in mitosis by establishment of the mitotic spindle which is the key element for chromosome alignment procedure; a macro structure called *kinetochore* guarantees the interactions between microtubules and the chromosomes^{26–28,30–33}.

Microtubules are made up of $\alpha\beta$ tubulin heterodimers, which organize a two dimensional sheet of tubulin in a three start helical structure¹⁶. The alfa subunits tend to link a beta in the longitudinal direction and an alfa in circumferential direction⁶³. The $\alpha\beta$ heterodimer is very steady and dimers connect head to tail to develop a protofilament. The protofilaments combine laterally creating a tube-like conformation^{16,63}.

In vivo and in vitro experiments confirm the force generation in cell even without interference of the motor proteins. This force generation is due to polymerization and depolymerization of the microtubules in the mitotic spindle^{16,23,24,47,48}. The maximum forces generated is lower than the equilibrium force which is completely independent of the polymerization mechanism¹⁶.

The hydrolysis of nucleotides-GDP bound to tubulin establishes a non-equilibrium functioning of the cytoskeleton and morphological flexibility of the cell⁶⁴. During prophase of the mitosis, microtubules polymerize in random directions from any spindle pole and could be stabilized if they catch the kinetochore; otherwise, they go under they go under catastrophic depolymerization, shrink back to the pole and then other microtubules start to elongate in random directions^{16,20}. GDP-tubulin has a more curved configuration which avoid it to place well in the microtubule lattice. It has a much higher critical concentration respect to GTP-tubulin. Therefore, high quantity of mechanical energy accumulates in the microtubule lattice through hydrolysis processes^{48,65}.

The plus end instability of MTs is considered to be a driving forces for chromosome movements.

The kinetochore which connects microtubules to chromosomes is composed of 10 different kinetochore proteins, called KMN 'network', which consists of **K**NL1 complex, the **M**IS12 complex and the **N**DC80 complex. Ndc80 complex interacts at the dimeric interface of α - and β - tubulins and effects on the MT dynamics by supporting straight MTs^{26,36}.

Kinetochore assembles constitutive centromere associated network (CCAN) and arrests the plus end of the MT. Lengthening and shortening of MTs originated from dynamic instability of MTs create force at the kinetochore and these forces move the chromosomes toward the metaphase plate. The stability of the junctions between kinetochore and plus end of microtubule is guaranteed by Ndc80 complex and by a W-shaped homodimer of coiled coils, called *Ska complex*, which is vital for a correct cell division in human cells and it is suggested to be analogue of the Dam1/DASH complex in metazoans³⁴⁻³⁷. The Ska complex is composed of three components: Ska1, Ska2, Ska3/Rama1. Characterizing the structure of the Ska complex and analyzing its influences on the MT binding in vitro and mitotic progression in vivo might explain the interdependency of the protein subunits of Ska complex and their role in the MT binding during cell division^{34,38,39}.

The MT-binding domains (MTBDs) of the Ska complex have transversal bindings with MTs and these connections are at the ends of W-shaped heterodimer. The symmetrical microtubule binding of the ska complex is vital in vivo^{34,41,43}. Ska1 (133-255) (called Ska1-MTBD) is the most efficient fragment of Ska complex, if dimerized. Ska1-MTBD is also required for primary chromosome alignment, mitotic progression and formation of the strong attachments between microtubule and kinetochore. It is about 5nm long and about 3nm wide³⁵⁻³⁷.

Human Ska complex binds MTs through several binding sites defined as "multipartite binding mode"³⁶. Analysis of the electrostatic surface potential demonstrated that on the surface of the Ska1-MTBD positive charges are present: the hypothesis that Ska complex identify MTs via polar connections take place^{35,36,66}.

In this work, protein-protein complexes of Ska1-MTBD and tubulin heterodimer were predicted and investigated by a coupled approach involving molecular docking techniques, to predict

possible Ska-Tubulin interacting complexes (based on experimental data and morphological and topological protein characters) and classical+steered Molecular Dynamics to shed light on force generation mechanisms in the kinetochore-microtubule junctions.

4.2 MATERIALS AND METHODS

4.2.1 System set up

The Human Ska1-MTBD (PDB ID: 4c9y) and Tubulin wall (PDB ID: 3j6f) were selected as template. By means of MODELLER and CHIMERA⁶⁷, the initial structures were improved and refined in particular for what concern missing residues in the 3j6f structure. In detail, for the α -tubulin missing residues (1, 39-48) and β -tubulin missing residues (1, 46-46, 361-368) were added. GTP and GDP ligands and Mg^{2+} ions were kept in the system structural model with the same relative positions with respect to the tubulin as defined in the 3j6f model.

ClusPro^{68,69} protein docking webserver was employed to predict possible interacting configurations between ska and tubulin models. In a greater detail, recent literature (in vitro mutation studies³⁶) indicated several interaction sites on the tubulin dimer and Ska1-MTBD³⁶. The table below shows the regions of experimentally revealed interaction residues between ska1 and tubulin monomers.

RECEPTOR	RECEPTOR RESIDUES	LIGAND (SKA1-MTBD) CLUSTER RESIDUES
<i>β Tubulin Cluster1</i>	<i>E110, E113, Y108</i>	<i>K52, K53, K72, K75</i> <i>R114</i>
		<i>K86, K92, K95, K96</i>
<i>β Tubulin Cluster2</i>	<i>E159, E160, Y161</i>	<i>K52, K53, K72, K75</i>
		<i>K86, K92, K95, K96</i>
<i>α Tubulin Cluster1</i>	<i>E423, D424, E429</i>	<i>K52, K53, K72, K75</i>

Table 4.1 Ska1MTBD cluster1: K52/53, cluster2: K72/75, cluster3: K86/92/95/96, cluster 4: R114.

The above mentioned experimentally highlighted interaction residues were considered to drive ClusPro docking procedure as already done in previous literature⁶⁸⁻⁷⁰. ClusPro executes three computational levels of modelling to perform the docking procedure (Figure 4.1): first employ a rigid body docking by sampling billions of protein-protein interacting conformations; then, finds the most probable models of the complex represented by most massive clusters applying root mean square deviation (RMSD) clustering on lowest energy conformations; finally through minimization performs a refinement and choose a certain number of significant output models⁶⁸⁻⁷².

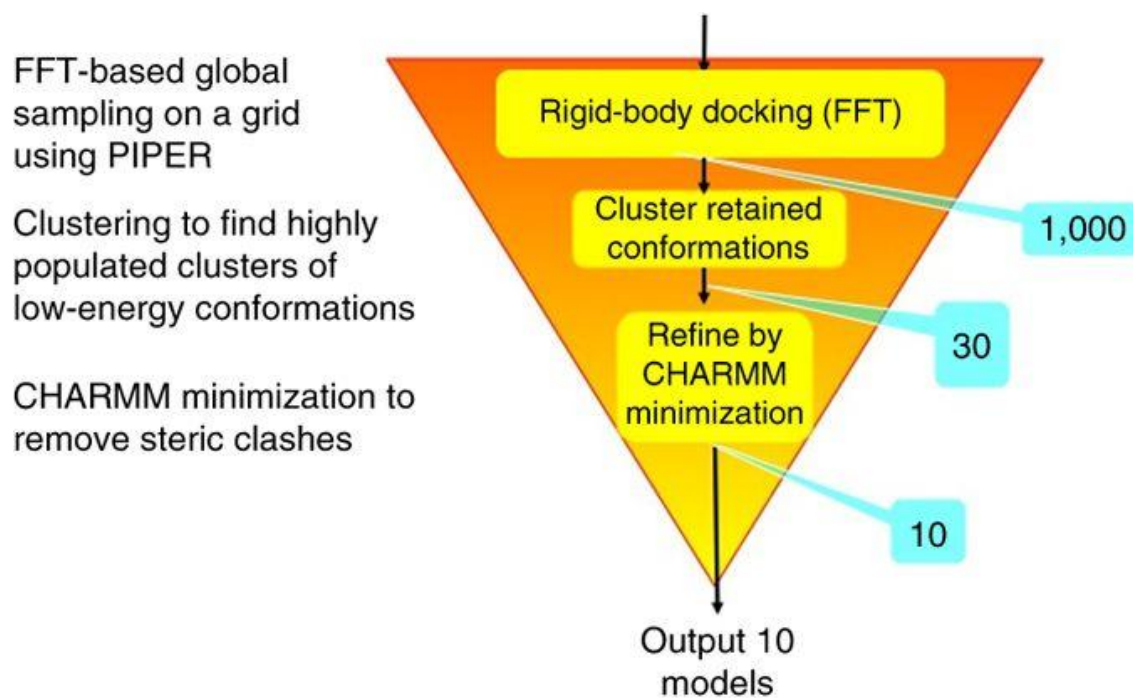


Figure 4.1. The blue boxes show the number of conformations maintained in each step of docking process⁶⁹.

Eight output models from ClusPro were considered as significant starting structures for further investigations by MD simulations.

4.2.2 Simulation Setup

GROMACS 2019.1⁷³ version was employed for molecular dynamics simulations of the models extracted from Cluspro. For each system protein topologies were established by the CHARMM36 force field and the TIP3P explicit water model was employed as solvent⁷⁴. Periodic boundary conditions were implemented with a dodecahedron box which surrounded the protein complex at the minimum distance of 0.65 nm. For neutralizing the charges, sodium and chlorine ions were added. Energy minimization for each system was performed applying steepest descent algorithm⁷⁴. The equilibration of the system was conducted first through velocity-rescale thermostat⁷⁵ in NVT ensemble to maintain the temperature at 300 K through 50 ps of simulation and then in NPT ensemble via velocity-rescale Berendsen barostat⁷⁶ for 500 ps to keep the pressure at 1 atm. To constrain the hydrogen bonds the LINCS algorithm was applied⁵⁴ and for the calculation of the electrostatic interactions Particle-mesh Ewald (PME) method defining a 1.2 nm cut-off⁵⁷ was used. After system equilibration, 20 ns of MD simulation was performed by 2 fs time step and the trajectories were saved every 2 ps. The Visual Molecular Dynamics (VMD) was used to represent the simulated systems⁷⁷.

Tubulin-Ska models were analyzed and successively simulated also by the steered molecular dynamics. To apply steered molecular dynamics, the tubulin heterodimer was constrained at a constant coordinate and an external potential was applied on Ska1-MTBD center of mass by a spring with the stiffness of $k=100 \text{ KJmol}^{-1}\text{m}^{-2}$ with a constant velocity of 0.01 nm/ps.

4.3 RESULTS

4.3.1 Conformational Analysis

ClusPro docked configurations are reported in Figure 4.2. Throughout the overall molecular Dynamics, no significant structural modifications were detected. This indicate that, as expected, predicted interacting models were stable during the overall dynamics.

Root Mean Square Deviation (RMSD) was calculated to distinguish if the 8 models are generally stable during simulation. As demonstrated in the Figure 4.3, the RMSD of the backbone atoms

with respect to the initial structures was calculated for the alfa tubulin, beta tubulin and ska proteins chains. Structural equilibrium is achieved in the last 5 ns of the overall trajectory.

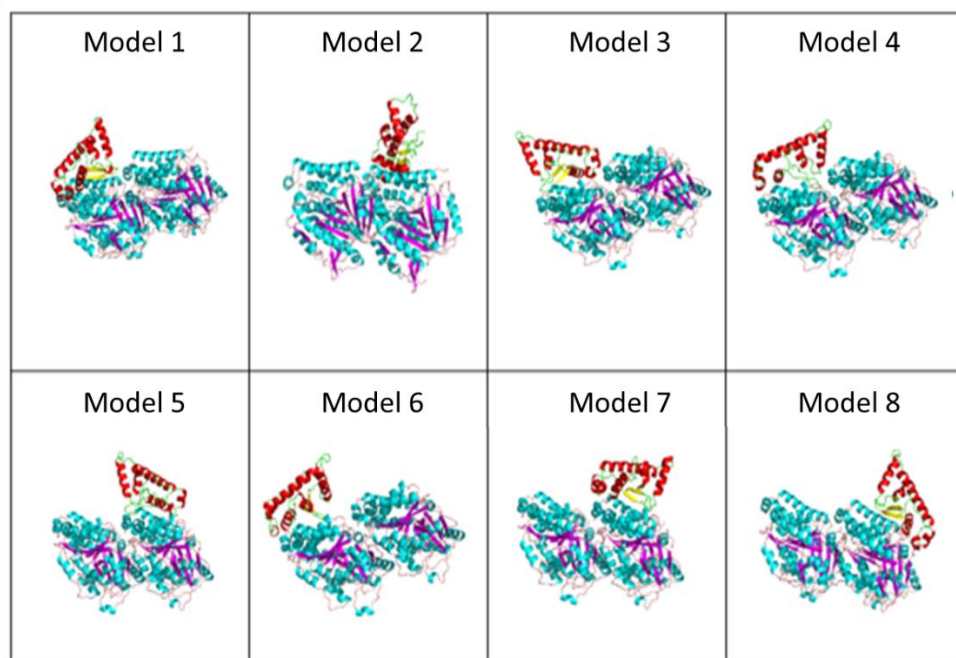


Figure 4.2 Eight different structures chosen by Cluspro as the conformations by lowest energy.

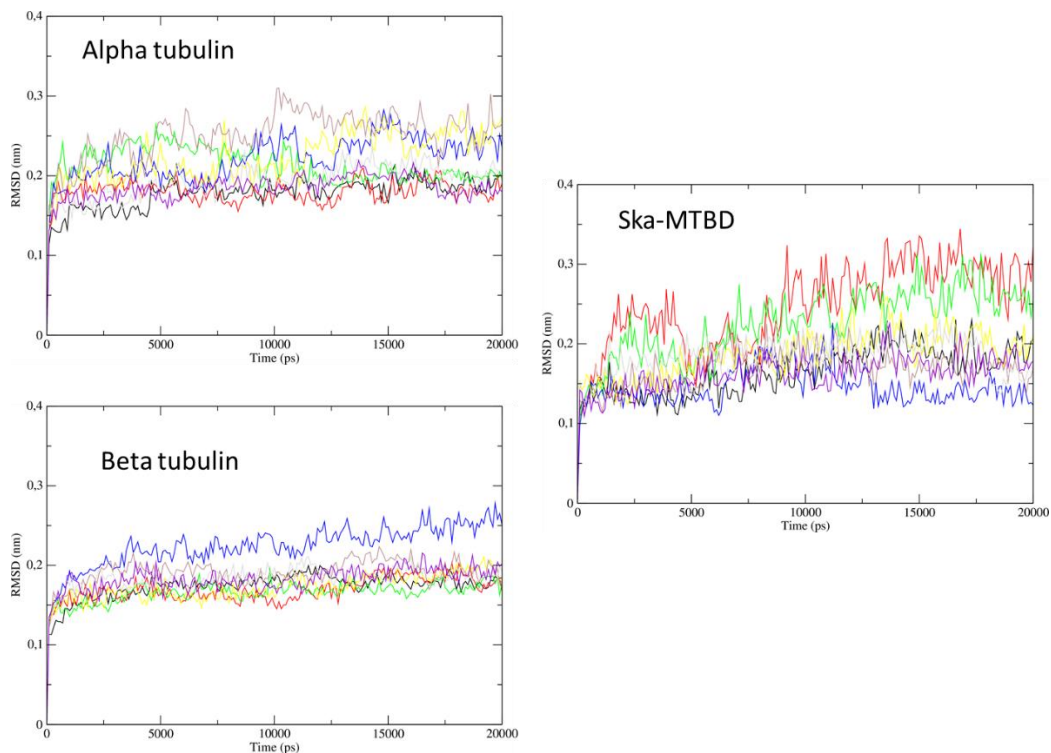


Figure 4.3 RMSD of *alfa tubulin*, *beta tubulin* and *Ska1-MTBD* for eight models throughout the overall MD simulations.

The secondary structure of Ska1-MTBD was investigated applying STRIDE^{42,78} for all eight models in the structural equilibrium time range. The probability of secondary structures is represented in figure 4.4 for each model. Also in this case, throughout the overall simulation, not significant effects on secondary structure are identified. Again this is a proof that the ska-tub contact is a stable interaction which does not destabilize the protein folding and probably mainly involves local phenomena of binding residue slight conformational changes.

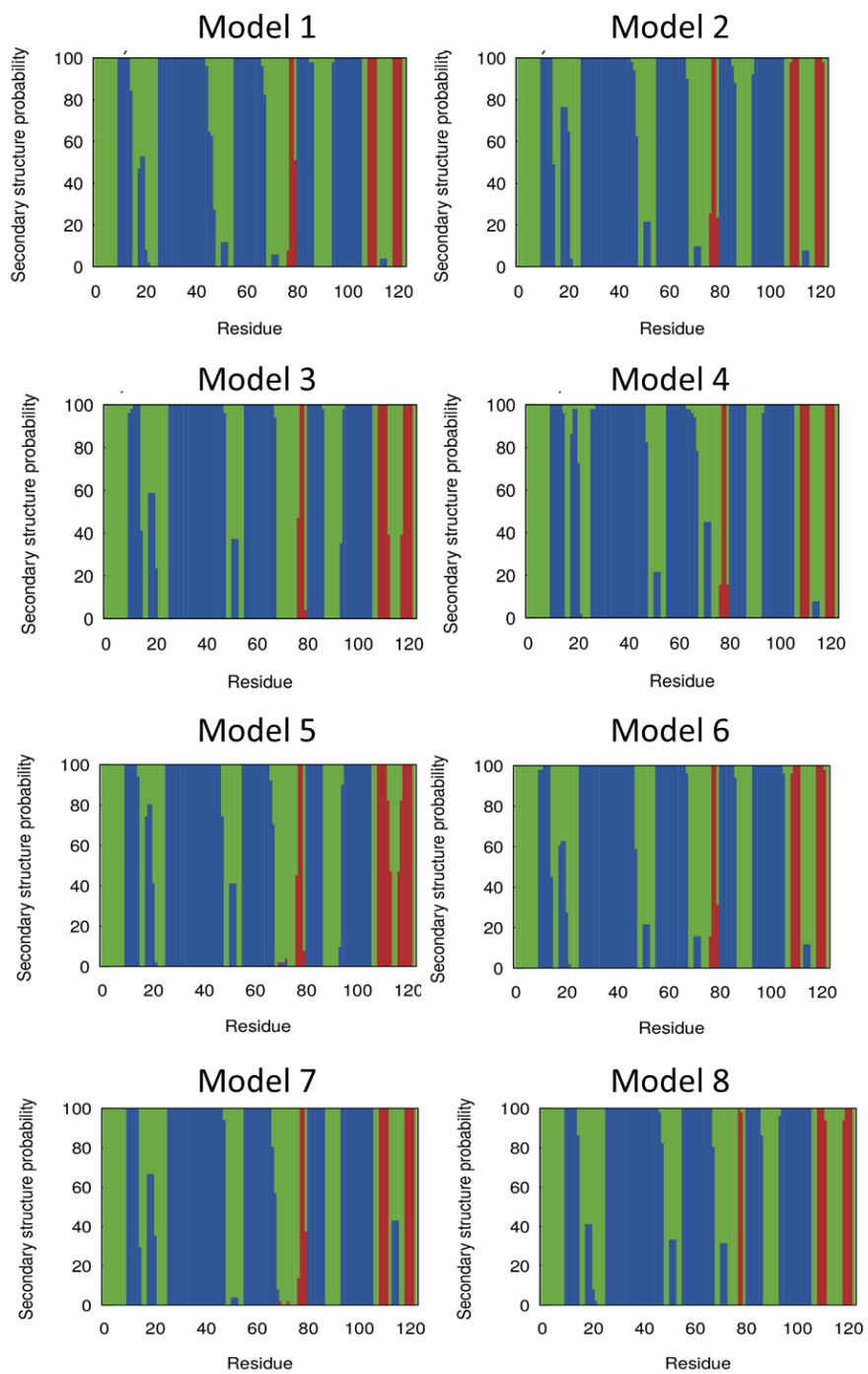


Figure 4.4 Secondary structure probability of Ska1-MTBD for eight models after MD simulations.

More information on local conformational changes are provided by fluctuations analysis (RMSF),

such as possible side chains conformationally rearrange due to binding (Figure 4.5). In addition, it would help discussing about possible correlations between fluctuation values and amino acids tendencies to each other between tubulin dimer and Ska1-MTBD⁷⁹. The Root Mean Square Fluctuations (RMSF) was analyzed by calculating the variations of C-alfa atoms respect to their average coordinates. These analyses demonstrate protein fluctuations per residue and characterizing the protein structure regarding local motions. The RMSF was obtained for each model, for simulated chains of alfa, beta and ska separately.

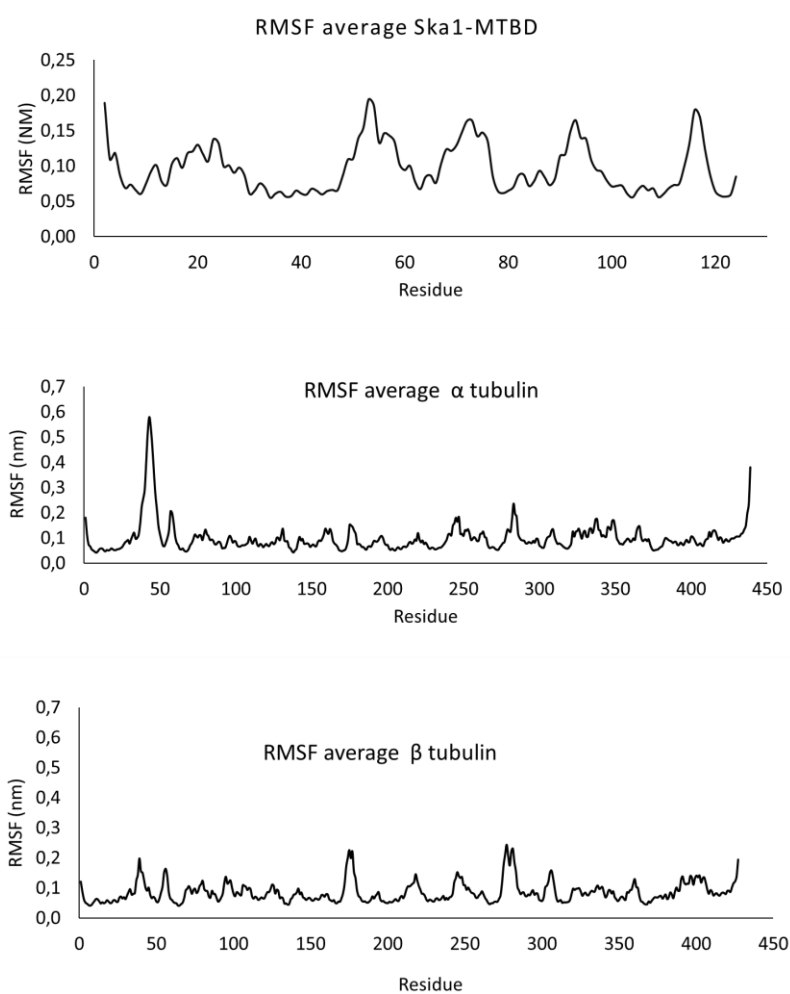


Figure 4.5 RMSD average fluctuations for six simulated models for a) ska, b) alfa and c) beta chain

For each model RMSF values clarify highly fluctuating residues. These local picks of fluctuation emerge following highly fluctuating residues for each group chain: on the alfa chain SER 38-SER 48 located in H1-S2 domain of tubulin, GLY 57, ALA 58 both in T1, HIS 283, GLU 284 in M-loop, and SER 439 at C-terminal are the highest fluctuating. These picks are mostly located on the coil or turn regions between alfa helices and beta sheets and particularly on the C-terminal. For the beta chain, instead, ASP 39 in H1-S2 , LYS 174, VAL 175, SER 176 all in T5, ARG 276, GLY277, SER 278, GLN 280, TYR281 all located in M-loop, are the picks of the fluctuations which again located mostly in the regions of turn or coil. The same observation on the ska chain shows that the highly fluctuated residues are: SER 2, LYS 52, LYS 53, SER 54 are located on α_4 and SER 57 on α_5 , LYS 72, ASP 73 on α_6 , LYS 92, ALA 93 are between α_7 and α_8 , GLY 116, GLY 117 are between β_2 and β_3 . It is worth noticing that the most fluctuating residues have been also highlighted in previous literature as related to ska-tub complex stability³⁶.

4.3.2 Interaction probability analysis

Contact Probability has been calculated between residues Ska1-MTBD and tubulin heterodimer. Contact probability for each residue was calculated using the following procedure described in⁸⁰. Trajectory snapshots were extracted in the last 5 ns of each MD simulation. For each snapshot the distance between a residue in a monomer and all residues of the interfacing monomer was calculated. If, at least one distance value among the residue-residue distances is equal or less than a chosen threshold (e.g., 0.28 or 0.6 nm), the residue was considered in contact with the interfacing monomer in that snapshot. The number of “contact snapshots” normalized over total snapshots is the contact probability associated with the residue. Figure 4.6 and 4.7 show the contact probability of all residues of ska and tubulin for each model separately with the value of cut-off equal to 0.28 nm and 0.6 nm. The residues with highest probability of interactions are SER19, CYS107, VAL113 and THR124 (the C-terminal): these domains are those which among different models have highest affinity to tubulin.

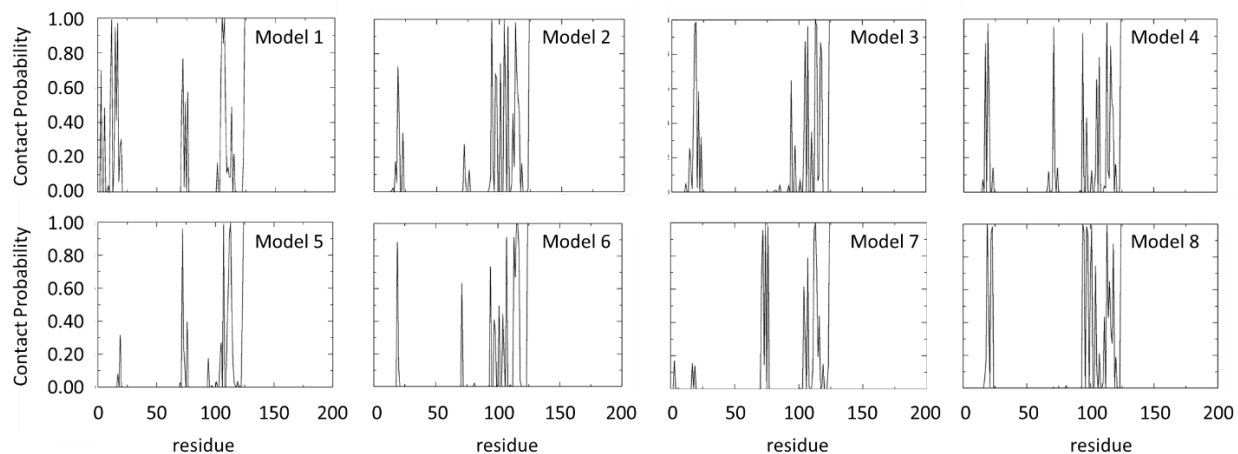


Figure 4.6 Contact probability values per residue for Ska1-MTBD calculated during the simulation for each model, the cut-off predefined at 0.28 nm.

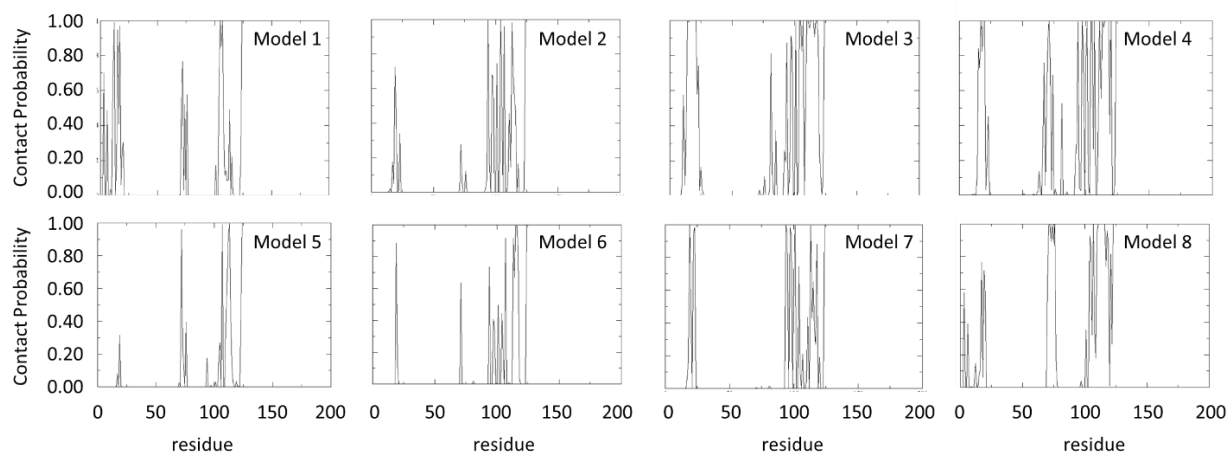


Figure 4.7 Contact probability values per residue for Ska1-MTBD calculated during the simulation for each model, the cut-off predefined at 0.6 nm.

Monitoring the contact probability at final 5 ns of the simulation is well noted that the residues with highest probability of interaction on Ska1-MTBD are SER19, CYS107, VAL113 and THR124 the C-terminal.

Analysis of probability interaction declared the binding sites of Ska1-MTBD with tubulin docked models. Based on experimental results we employed in this computational research, the critical residues of Ska1-MTBD locate in the following domains: A1 (residue 50-55), A2 (residue 70-75), A3 (residue 83-89), A4 (residue 90-100) and A5 (residue 110-120).

The results of contact probability for cutoff value 0.28 nm and 0.6 nm for all models of Ska1-MTBD and tubulin complexes were controlled considering a threshold value of 0.8 for contact probability. We considered those residues which interact with a probability higher than 0.8. The analysis of probability interactions reveals the role of three domains of A2 (residue 70-75), A4 (residue 90-100) and A5 (residue 110-120) in the ska-tubulin attachment, among them A5 (residue 110-120) is the region of intense interactions, taking into account, the strict limit of cutoff equal to 0.28 nm. It is also observed the noninterference of A1 (residue 50-55) and A3 (residue 83-89); the residues of these two domains do not exhibit interactions with tubulin heterodimers in none of our Ska1-MTBD and tubulin complexes (table 4.2).

Table 4.2 shows also that changing the cutoff from 0.28 nm to 0.6 nm changes very little the domain involvement in the binding. This means that the ska areas playing role in the ska-tub interaction participate to the binding with primary interactions, very close to the tubulin surface.

Table 4.2 This table shows the binding sites (A1 (residue 50-55), A2 (residue 70-75), A3 (residue 83-89), A4 (residue 90-100) and A5 (residue 110-120) statistics of interactions by contact probability calculation with a threshold of 0.8 for contact probability. Two cutoff value of 0.6 nm and 0.28 were confronted to reveal the more critical residues.

Binding Region	Probability of Interaction in the 8 predicted ska-tub complexes	
	Cutoff 0.28 nm	Cutoff 0.6 nm
A1	0%	0%
A2	50%	75%
A3	0%	0%
A4	38%	63%
A5	88%	100%

4.3.3 Steered Molecular Dynamics

The eight models after molecular dynamics has been investigated via steered molecular dynamics (SMD) to study the detachment force of Ska1-MTBD from tubulin. The pulling was applied only in one direction with a constant velocity. The stress vs strain curves (Figure 4.8 left) illustrate that the displacement abruptly increases for all models at onset of the force. The stress vs. strain curves follows a progress composed by regions with different slopes. In general a linear behaviour can be always identified. In this region the elastic modulus can be calculated.

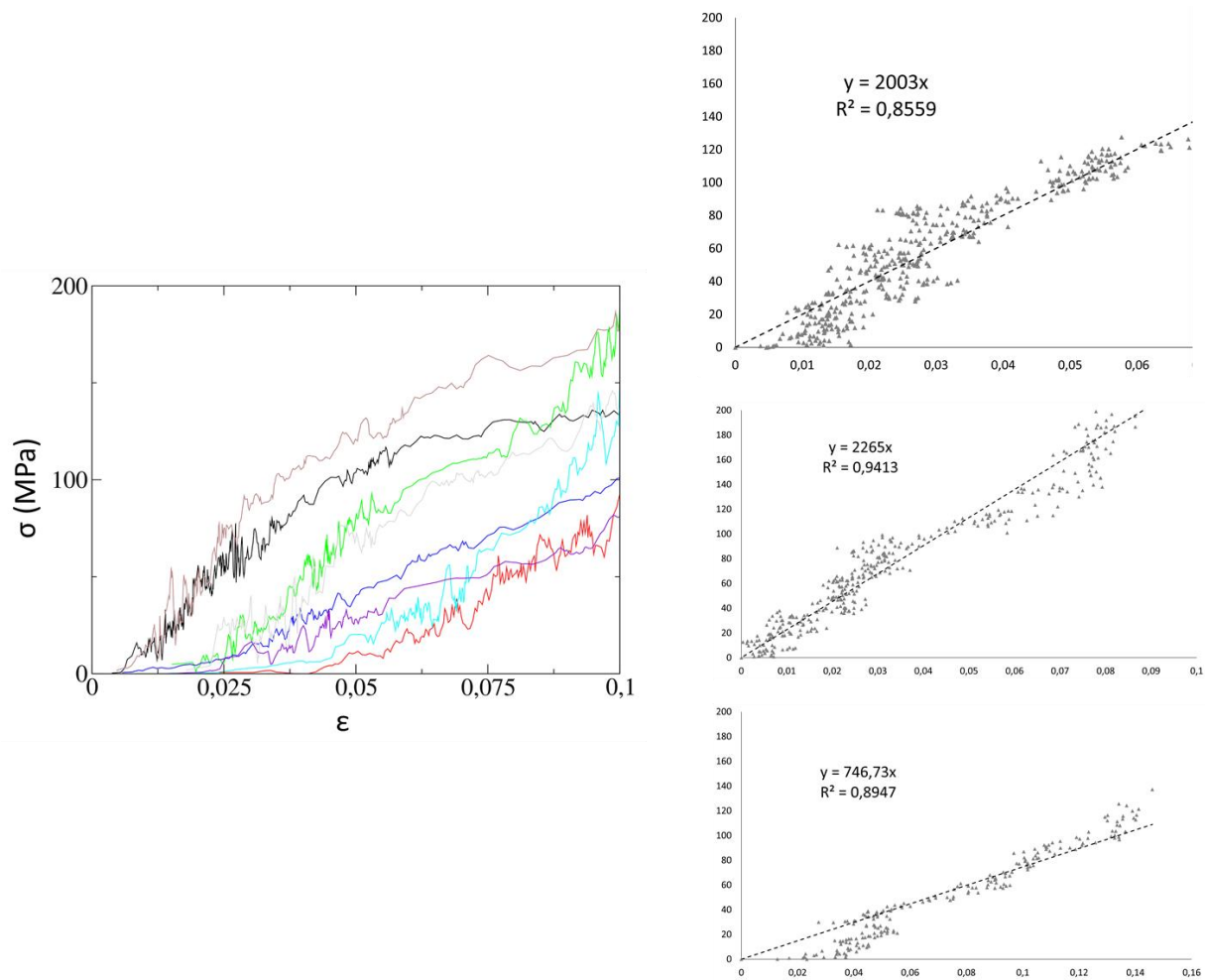


Figure 4.8 (Left), Stress strain curves for the 8 ska-tub complex configurations considered in this work.

Moreover, every curve shows increments until the protein complex detachment is initialized and then the force becomes approximately constant and reaches a plateau. At the yield point which finishes the elastic deformation region, ska initiates a sort of plastic deformation until being completely detached from tubulin. Curves with higher slope for deformation range 0-5% are representative of those models characterized by the strongest ska-tub binding affinity. In a greater detail the highest Young modulus was found for model 1 ($Y=2\text{GPa}$), in agreement with the rank provided by ClusPro.

4.4 DISCUSSION

Classical molecular dynamics simulation results exhibit various information about the binding sites, in the complex of Ska1-MTBD and the tubulin heterodimer. The RMSF results reveal information about the highest fluctuating residues of ska, alfa and beta tubulin. Analyzing the fluctuation of alfa and beta chains it is noted that picks of fluctuations generally occur in residues which are located on the coil or turn regions between alfa helices and beta sheets and particularly on the C-terminal.

To perform a more accurate analysis about the interacting sites of the ska tubulin complex, the contact probability of all residues was calculated to reveal the residues which are inside a 0.28 nm cut-off value. The analysis of contact probability was investigated defining five domains of ska residues based on residues which were demonstrated to be critical in bindings with tubulin³⁶. The eight models were studied to unveil the more interacting domains of ska bound to tubulin. This analysis supports the experimental results³⁶ considering three domains of ska: A2 (residue 70-75) with coil secondary structures, A4 (residue 90-100) with coil and alfa helix structure and A5 (residue 110-120) with coil and beta sheet structures, with the highest probability of interaction (more than 0.8)

Steered MD results revealed the stress-strain curves which demonstrate in general an elastic regime followed by a plastic deformations in all eight models. Steered molecular dynamics results disclosed the first model of ClusPro (the model with lowest energy) as the complex of ska and tubulin with the highest affinity of the tubulin for the ska because the rupture event was evidently

later respect to other models after being simulated via SMD and applying the same external force by the spring of $100 \text{ KJ mol}^{-1}\text{nm}^{-2}$ with the same velocity of unbinding on all eight models. Comparing the strain-stress curves we observe that the first model which is the one with highest affinity of ska for tubulin shows a more accurate linear progress in the first zone. Throughout this elastic procedure, the ska backbone continues to be strained in the direction of pulling and becomes extended respect to the initial conformation at the beginning of the SMD. This conformational development provokes rupture by transforming hydrogen and electrostatic bonding⁴³. It is of interest that the best model predicted by ClusPro (ranked first) is also the one with the highest Elastic modulus ($Y=2\text{GPa}$). It is worth mentioning that this identified strength of ska-tub interaction is comparable with mechanical properties exhibited by tubulin dimers and other proteins such as amyloid fibrils⁸¹⁻⁸³.

5 CONCLUSIONS

Mitotic spindle is a complex structure which perform chromosome segregation during mitosis. It is composed of microtubules, hollow cylindrical polar filaments. The dynamic instability of microtubules is the driving force of chromosome segregation. Proper chromosome segregation depends on the stability of the kinetochore-microtubule junctions which is guaranteed by the interference of Ska complex. The investigations about force generation in mitotic spindle has been accelerated in recent decades thanks to immense computer hardware and software upgrades which manage to model enormous biological structures with huge number of molecules.

In this work, the most updated biochemical experimental results have been employed to initiate the computational and molecular modelling inspections on the stability of the kinetochore-microtubules attachments. The classical and steered molecular dynamics methods were implemented for simulations of microtubule binding domains of Ska complex in the context of protein-protein docked configurations with $\alpha\beta$ -tubulin heterodimer, achieved by protein-protein docking. The results of this present research approved the high probability of interactions between binding domains of Ska complex which experimentally were demonstrated to be crucial.

Among these five critical domains three were absolutely attached with the contact probability higher than 0.8 even with a strict cutoff value equal to 0.28 nm. The steered molecular dynamics analysis leads us to calculate the detachment force of Ska1-MTBD from tubulin.

The future computational efforts might be applied to investigate more details on the interactions between Ska complex and microtubules. Considering the complexity of the elements for molecular dynamics simulations, is necessary to optimize the modality in which tubulin dimers are configurated, for example a ring structure of protofilaments might be the most efficient to proceed ahead.

6 Acknowledgments

I would like to show my gratitude to my supervisor Prof. Jacek Adam Tuszynski

I would like to thank my co-supervisor Prof. Marco Agostino Deriu for giving me the opportunity to work on this thesis and for supporting me in every moment; his enthusiasm and professionalism made this research work very exciting and constantly increased my interest in molecular modeling.

I would also thank Lorenzo Pallante for important hints and explanations, especially about dimensionality reduction techniques.

I finally thank my family for constantly encouraging me and all my friends for always being there.

7 References

1. Civelekoglu-Scholey G, Cimini D. Modelling chromosome dynamics in mitosis: A historical perspective on models of metaphase and anaphase in eukaryotic cells. *Interface Focus*. 2014;4(3). doi:10.1098/rsfs.2013.0073
2. Oriola D, Needleman DJ, Brugués J. The Physics of the Metaphase Spindle. *Annu Rev Biophys*. 2018;47(1):655-673. doi:10.1146/annurev-biophys-060414-034107
3. Shtylla B, Keener JP. A mechanomolecular model for the movement of chromosomes during mitosis driven by a minimal kinetochore bicyclic cascade. *J Theor Biol*. 2010;263(4):455-470. doi:10.1016/j.jtbi.2009.12.023
4. Howard J, Hyman AA. Dynamics and mechanics of the microtubule plus end. *Nature*. 2003;422(6933):753-758. doi:10.1038/nature01600
5. Desai A, Mitchison TJ. MICROTUBULE POLYMERIZATION DYNAMICS. *Annu Rev Cell Dev Biol*. 1997;13(1):83-117. doi:10.1146/annurev.cellbio.13.1.83
6. Siegrist S, development CD-G&, 2007 undefined. Microtubule-induced cortical cell polarity. *genesdev.cshlp.org*. <http://genesdev.cshlp.org/content/21/5/483.short>. Accessed July 8, 2019.
7. Gadde S, Biology RH-C, 2004 undefined. Mechanisms and molecules of the mitotic spindle. *Elsevier*. <https://www.sciencedirect.com/science/article/pii/S0960982204006979>. Accessed July 8, 2019.
8. Larson ME, Harrison BD, Bloom K. Biochimie Uncovering chromatin ' s contribution to the mitotic spindle : Applications of computational and polymer models. *Biochimie*. 2010;92(12):1741-1748. doi:10.1016/j.biochi.2010.06.014
9. Walczak CE, Cai S, Khodjakov A. Mechanisms of chromosome behaviour during mitosis. *Nat Rev Mol Cell Biol*. 2010;11(2):91-102. doi:10.1038/nrm2832

10. Nogales E, Wolf SG, Downing KH. Erratum: Structure of the $\alpha\beta$ tubulin dimer by electron crystallography. *Nature*. 1998;393(6681):191-191. doi:10.1038/30288
11. Löwe J, Li H, Downing K., Nogales E. Refined structure of $\alpha\beta$ -tubulin at 3.5 Å resolution. *J Mol Biol*. 2001;313(5):1045-1057. doi:10.1006/JMBI.2001.5077
12. Nogales E, Wolf SG, Downing KH. Electron Crystallography. 1998;391(January):199-204.
13. Alushin GM, Lander GC, Kellogg EH, Zhang R, Baker D, Nogales E. High-Resolution microtubule structures reveal the structural transitions in $\alpha\beta$ -tubulin upon GTP hydrolysis. *Cell*. 2014;157(5):1117-1129. doi:10.1016/j.cell.2014.03.053
14. Aprodu I, Soncini M, Redaelli A. Interaction forces and interface properties of KIF1A kinesin- $\alpha\beta$ tubulin complex assessed by molecular dynamics. *J Biomech*. 2008;41(15):3196-3201. doi:10.1016/j.jbiomech.2008.08.014
15. Erickson HP. Protofilaments and rings, two conformations of the tubulin family conserved from bacterial FtsZ to alpha/beta and gamma tubulin. *J Cell Biol*. 1996;135(1):5-8. doi:10.1083/jcb.135.1.5
16. Howard J. Mechanics of Motor Proteins and the Cytoskeleton About the Author (s). 2001;3344.
17. Pilhofer M, Ladinsky MS, McDowall AW, Petroni G, Jensen GJ. Microtubules in Bacteria: Ancient Tubulins Build a Five-Protofilament Homolog of the Eukaryotic Cytoskeleton. Amos L, ed. *PLoS Biol*. 2011;9(12):e1001213. doi:10.1371/journal.pbio.1001213
18. Grafmüller A, Noya EG, Voth GA. Nucleotide-Dependent Lateral and Longitudinal Interactions in Microtubules. *J Mol Biol*. 2013;425(12):2232-2246. doi:10.1016/J.JMB.2013.03.029
19. Hawkins T, Mirigian M, Selcuk Yasar M, Ross JL. Mechanics of microtubules. *J Biomech*. 2010;43(1):23-30. doi:10.1016/j.jbiomech.2009.09.005
20. Mandelkow EM, Mandelkow E, Milligan RA. Microtubule dynamics and microtubule caps:

- A time-resolved cryo-electron microscopy study. *J Cell Biol.* 1991;114(5):977-991.
doi:10.1083/jcb.114.5.977
21. Cassimeris LU, Walker RA, Pryer NK, Salmon ED. Dynamic instability of microtubules. *BioEssays.* 1987;7(4):149-154. doi:10.1002/bies.950070403
 22. Mitchison T, nature MK-, 1984 undefined. Dynamic instability of microtubule growth. *nature.com.* <https://www.nature.com/articles/312237a0>. Accessed July 8, 2019.
 23. Elting MW, Hueschen CL, Udy DB, Dumont S. Force on spindle microtubule minus ends moves chromosomes. *J Cell Biol.* 2014;206(2):245-256. doi:10.1083/jcb.201401091
 24. Umbreit NT, Davis TN. Mitosis puts sisters in a strained relationship: Force generation at the kinetochore. *Exp Cell Res.* 2012;318(12):1361-1366. doi:10.1016/j.yexcr.2012.04.008
 25. Vukušić K, Buđa R, Bosilj A, Milas A, Pavin N, Tolić IM. Microtubule Sliding within the Bridging Fiber Pushes Kinetochore Fibers Apart to Segregate Chromosomes. *Dev Cell.* 2017;43(1):11-23.e6. doi:10.1016/j.devcel.2017.09.010
 26. DeLuca JG, Musacchio A. Structural organization of the kinetochore-microtubule interface. *Curr Opin Cell Biol.* 2012;24(1):48-56. doi:10.1016/j.ceb.2011.11.003
 27. Santaguida S, Musacchio A. The life and miracles of kinetochores. *EMBO J.* 2009;28(17):2511-2531. doi:10.1038/emboj.2009.173
 28. Bertalan Z, La Porta CAM, Maiato H, Zapperi S. Conformational mechanism for the stability of microtubule-kinetochore attachments. *Biophys J.* 2014;107(2):289-300. doi:10.1016/j.bpj.2014.06.004
 29. Torino PDI. as drug delivery systems for anticancer. 2019.
 30. Ciferri C, Pasqualato S, Screpanti E, et al. Implications for Kinetochore-Microtubule Attachment from the Structure of an Engineered Ndc80 Complex. *Cell.* 2008;133(3):427-439. doi:10.1016/j.cell.2008.03.020
 31. Powers AF, Franck AD, Gestaut DR, et al. The Ndc80 Kinetochore Complex Forms Load-

- Bearing Attachments to Dynamic Microtubule Tips via Biased Diffusion. *Cell*. 2009;136(5):865-875. doi:10.1016/j.cell.2008.12.045
32. Alushin GM, Ramey VH, Pasqualato S, et al. The Ndc80 kinetochore complex forms oligomeric arrays along microtubules. *Nature*. 2010;467(7317):805-810. doi:10.1038/nature09423
 33. Cheerambathur DK, Desai A. Linked in: Formation and regulation of microtubule attachments during chromosome segregation. *Curr Opin Cell Biol*. 2014;26(1):113-122. doi:10.1016/j.ceb.2013.12.005
 34. Jeyaprakash AA, Santamaria A, Jayachandran U, et al. Structural and Functional Organization of the Ska Complex, a Key Component of the Kinetochore-Microtubule Interface. *Mol Cell*. 2012;46(3):274-286. doi:10.1016/j.molcel.2012.03.005
 35. Schmidt JC, Arthanari H, Boeszoermyeni A, et al. The Kinetochore-Bound Ska1 Complex Tracks Depolymerizing Microtubules and Binds to Curved Protofilaments. *Dev Cell*. 2012;23(5):968-980. doi:10.1016/j.devcel.2012.09.012
 36. Abad MA, Medina B, Santamaria A, et al. Structural basis for microtubule recognition by the human kinetochore Ska complex. *Nat Commun*. 2014;5:1-14. doi:10.1038/ncomms3964
 37. Welburn JPI, Grishchuk EL, Backer CB, Wilson-Kubalek EM, Yates JR, Cheeseman IM. The Human Kinetochore Ska1 Complex Facilitates Microtubule Depolymerization-Coupled Motility. *Dev Cell*. 2009;16(3):374-385. doi:10.1016/j.devcel.2009.01.011
 38. Guimaraes GJ, Deluca JG. Connecting with Ska, a key complex at the kinetochore-microtubule interface. *EMBO J*. 2009;28(10):1375-1377. doi:10.1038/emboj.2009.124
 39. Abad MA, Zou J, Medina-Pritchard B, et al. Ska3 Ensures Timely Mitotic Progression by Interacting Directly with Microtubules and Ska1 Microtubule Binding Domain. *Sci Rep*. 2016;6(June):1-9. doi:10.1038/srep34042
 40. Helgeson LA, Zelter A, Riffle M, MacCoss MJ, Asbury CL, Davis TN. Human Ska complex

- and Ndc80 complex interact to form a load-bearing assembly that strengthens kinetochore–microtubule attachments. *Proc Natl Acad Sci*. 2018;115(11):2740-2745. doi:10.1073/pnas.1718553115
41. Janczyk P, Skorupka KA, Tooley JG, et al. Mechanism of Ska Recruitment by Ndc80 Complexes to Kinetochores. *Dev Cell*. 2017;41(4):438-449.e4. doi:10.1016/j.devcel.2017.04.020
 42. Monda JK, Whitney IP, Tarasovets E V., et al. Microtubule Tip Tracking by the Spindle and Report Microtubule Tip Tracking by the Spindle and Kinetochore Protein Ska1 Requires Diverse Tubulin-Interacting Surfaces. *Curr Biol*. 2017;27(23):3666-3675.e6. doi:10.1016/j.cub.2017.10.018
 43. Zhang G, Kelstrup CD, Hu X, et al. Accepted manuscript The Ndc80 internal loop is required for recruitment of the Ska complex to establish end-on microtubule attachment to. *Heal (San Fr*. 2012;(March).
 44. Zhang Q, Sivakumar S, Chen Y, et al. Ska3 Phosphorylated by Cdk1 Binds Ndc80 and Recruits Ska to Kinetochores to Promote Mitotic Progression. *Curr Biol*. 2017;27(10):1477-1484.e4. doi:10.1016/j.cub.2017.03.060
 45. Kirschner MW. Implications of Treadmilling for the Stability and Polarity of Actin and Tubulin Polymers In Vivo The Critical Concentration for Bidirectional Growth. *J Cell Biol*. 1980;86(20):0-4.
 46. Moores CA. Lucky 13 - microtubule depolymerisation by kinesin-13 motors. *J Cell Sci*. 2006;119(19):3905-3913. doi:10.1242/jcs.03224
 47. Med CC. 氢气和蛛网膜下腔出血HHS Public Access. 2015;40(4):1291-1296. doi:10.1097/CCM.0b013e31823da96d.Hydrogen
 48. Molodtsov MI, Grishchuk EL, Efremov AK, McIntosh JR, Ataullakhanov FI. Force production by depolymerizing microtubules: A theoretical study. *Proc Natl Acad Sci*. 2005;102(12):4353-4358. doi:10.1073/pnas.0501142102

49. McCammon JA, Gelin BR, Karplus M. Dynamics of folded proteins. *Nature*. 1977;267(5612):585-590. doi:10.1038/267585a0
50. Amadei A, Linssen AB, Berendsen HJ. Essential dynamics of proteins. *Proteins*. 1993;17(4):412-425. doi:10.1002/prot.340170408
51. Merszalek PE, Lu H, Li H, et al. Mechanical Unfolding intermediates in titin modules. *Nature*. 1999;402(November):4-7.
52. Lu H, Isralewitz B, Krammer a, Vogel V, Schulten K. Unfolding of titin immunoglobulin domains by steered molecular dynamics simulation. *Biophys J*. 1998;75(2):662-671. doi:10.1016/S0006-3495(98)77556-3
53. Elber R. Long-timescale simulation methods. *Curr Opin Struct Biol*. 2005;15(2):151-156. doi:10.1016/J.SBI.2005.02.004
54. Hess B, Bekker H, Berendsen HJC, Fraaije JGEM. LINCS: A linear constraint solver for molecular simulations. *J Comput Chem*. 1997;18(12):1463-1472. doi:10.1002/(SICI)1096-987X(199709)18:12<1463::AID-JCC4>3.0.CO;2-H
55. Leach AR. *Molecular Modelling : Principles and Applications*. Prentice Hall; 2001. https://books.google.it/books?hl=en&lr=&id=kB7jsbV-uhkC&oi=fnd&pg=PR9&dq=+Leach,+A.+R.+Molecular+modelling+:+principles+and+applications&ots=-_wpc0koIU&sig=6OtCQj7SiUzPPzxKp75pyZ5UA84#v=onepage&q=Leach%2CA. R. Molecular modelling %3A principles and applications&f=false. Accessed July 10, 2019.
56. Darden T, York D, Pedersen L. Particle mesh Ewald: An $N \cdot \log(N)$ method for Ewald sums in large systems. *J Chem Phys*. 1993;98(12):10089-10092. doi:10.1063/1.464397
57. Darden T, York D, Pedersen L. Particle mesh Ewald: An $N \cdot \log(N)$ method for Ewald sums in large systems. *J Chem Phys*. 1993;98(12):10089. doi:10.1063/1.464397
58. Cranford SW, Ortiz C, Buehler MJ. Mechanomutable properties of a PAA/PAH polyelectrolyte complex: Rate dependence and ionization effects on tunable adhesion

- strength. *Soft Matter*. 2010;6(17):4175-4188. doi:10.1039/c0sm00095g
59. Park S, Sculten K. Calculating potentials of mean force from steered molecular dynamics simulations. *J Chem Phys*. 2004;120(13):5946-5961. doi:10.1063/1.1651473
 60. Jarzynski C. Nonequilibrium Equality for Free Energy Differences. *Phys Rev Lett*. 1997;78(14):2690-2693. doi:10.1103/PhysRevLett.78.2690
 61. Jarzynski C. Equilibrium free-energy differences from nonequilibrium measurements: A master-equation approach. *Phys Rev Lett*. 1997;56(5):5018-5035. doi:10.1103/PhysRevE.56.5018
 62. Hess B, Kutzner C, van der Spoel D, Lindahl E. GROMACS 4: Algorithms for Highly Efficient, Load-Balanced, and Scalable Molecular Simulation. *J Chem Theory Comput*. 2008;4(3):435-447. doi:10.1021/ct700301q
 63. Erickson HP, Stoffler D. Protofilaments and Rings, Two Conformations of the Tubulin Family Conserved from Bacterial FtsZ to alpha/beta and gamma Tubulin. *October*. 1996;135(1):5-8.
 64. Howard J, Hyman A a. Dynamics and mechanics of the microtubule plus end. *Nature*. 2003;422(6933):753-758. doi:10.1038/nature01600
 65. Howard J. *Mechanics of Motor Proteins and the Cytoskeleton*. Vol 7.; 2001. doi:10.1017/CBO9781107415324.004
 66. Monda JK, Whitney IP, Tarasovetc E V., et al. Microtubule Tip Tracking by the Spindle and Kinetochore Protein Ska1 Requires Diverse Tubulin-Interacting Surfaces. *Curr Biol*. 2017;27(23):3666-3675.e6. doi:10.1016/j.cub.2017.10.018
 67. Yang Z, Lasker K, Schneidman-Duhovny D, et al. UCSF Chimera, MODELLER, and IMP: An integrated modeling system. *J Struct Biol*. 2012;179(3):269-278. doi:10.1016/j.jsb.2011.09.006
 68. Vajda S, Yueh C, Beglov D, et al. New additions to the ClusPro server motivated by CAPRI.

- Proteins Struct Funct Bioinforma*. 2017;85(3):435-444. doi:10.1002/prot.25219
69. Kozakov D, Hall DR, Xia B, et al. The ClusPro web server for protein–protein docking. *Nat Protoc*. 2017;12(2):255-278. doi:10.1038/nprot.2016.169
 70. Janin J, Henrick K, Moult J, et al. CAPRI: A critical assessment of PRedicted interactions. *Proteins Struct Funct Genet*. 2003;52(1):2-9. doi:10.1002/prot.10381
 71. Vajda S. Classification of protein complexes based on docking difficulty. *Proteins Struct Funct Genet*. 2005;60(2):176-180. doi:10.1002/prot.20554
 72. Xia B, Vajda S, Kozakov D. Supplementary Information for Accounting for pairwise distance restraints in FFT based protein-protein docking. 2013;2004.
 73. Abraham MJ, Murtola T, Schulz R, et al. GROMACS: High performance molecular simulations through multi-level parallelism from laptops to supercomputers. *SoftwareX*. 2015;1-2:19-25. doi:10.1016/j.softx.2015.06.001
 74. Jorgensen WL, Chandrasekhar J, Madura JD, Impey RW, Klein ML. Comparison of simple potential functions for simulating liquid water. *J Chem Phys*. 1983;79(2):926. doi:10.1063/1.445869
 75. Bussi G, Donadio D, Parrinello M. Canonical sampling through velocity rescaling. *J Chem Phys*. 2007;126(1):014101. doi:10.1063/1.2408420
 76. Berendsen HJC, Postma JPM, van Gunsteren WF, DiNola A, Haak JR. Molecular dynamics with coupling to an external bath. *J Chem Phys*. 1984;81(8):3684-3690. doi:10.1063/1.448118
 77. Humphrey W, Dalke A, graphics KS-J of molecular, 1996 undefined. VMD: visual molecular dynamics. *Elsevier*.
<https://www.sciencedirect.com/science/article/pii/0263785596000185>. Accessed July 6, 2019.
 78. Heinig M, Frishman D. STRIDE: a web server for secondary structure assignment from

- known atomic coordinates of proteins. *Nucleic Acids Res.* 2004;32(Web Server issue):W500-W502. doi:10.1093/nar/gkh429
79. RUVINSKY AM, KIRYS T, TUZIKOV A V., VAKSER IA. Structure Fluctuations and Conformational Changes in Protein Binding. *J Bioinform Comput Biol.* 2012;10(02):1241002. doi:10.1142/s0219720012410028
 80. Deriu MA, Grasso G, Licandro G, et al. Investigation of the Josephin Domain Protein-Protein Interaction by Molecular Dynamics. Salahub D, ed. *PLoS One.* 2014;9(9):e108677. doi:10.1371/journal.pone.0108677
 81. Enemark SS, Deriu MA, Soncini M, Redaelli A. Mechanical Model of the Tubulin Dimer Based on Molecular Dynamics Simulations. *J Biomech Eng.* 2008;130(4):041008-041008. doi:10.1115/1.2913330
 82. Deriu MA, Enemark S, Soncini M, Montevecchi FM, Redaelli A. Tubulin: from atomistic structure to supramolecular mechanical properties. *J Mater Sci.* 2007;42(21):8864-8872. doi:10.1007/s10853-007-1784-6
 83. Grasso G, Rebella M, Morbiducci U, Tuszynski JA, Danani A, Deriu MA. The Role of Structural Polymorphism in Driving the Mechanical Performance of the Alzheimer's Beta Amyloid Fibrils. *Front Bioeng Biotechnol.* 2019;7:83. doi:10.3389/fbioe.2019.00083

